Translating an open-ocean biogeochemistry code with cryptic sulfur cycling to Chesapeake Bay requires considering the impacts of burial, dissolved organic matter, and optics

Rui Jin[1], Marie-Aude Pradal[1], Kalev Hantsoo[1], Anand Gnanadesikan[1], Pierre St-Laurent[2], Christian J. Bjerrum[3]

1: Department of Earth and Planetary Sciences, Johns Hopkins University, Baltimore, Maryland, USA

2: Virginia Institute of Marine Science, William & Mary, Gloucester Point, Virginia, USA

3: Department of Geoscience and Natural Resource Management, University of Copenhagen, Copenhagen, DK

Correspondence: Rui Jin (ruijin@jhu.edu)

Abstract

A number of models have been developed to simulate hypoxia in the Chesapeake Bay, but these models do not agree on what processes must be included. In this study we implemented a previously published biogeochemical (BGC) code developed for open-ocean waters that includes “cryptic” microbial sulfur cycling, a process that can increase denitrification and anammox rates in anoxic waters. We ran this BGC code within the ChesROMS physical model of the Chesapeake Bay, then compared the results to those of a ChesROMS simulation with an estuarine BGC code previously implemented and calibrated in the Bay. The estuarine BGC code neglects sulfur cycling but includes burial of particulate organic matter (POM) and cycling

of dissolved organic matter (DOM) and uses different values for many parameters governing phytoplankton growth and particle dynamics. At a key test site (the Bay Bridge Station), the model with sulfur cycling gives better results for oxygen and nitrate. However, it also gives a worse overprediction of ammonium—suggesting that its greater accuracy in predicting these two variables may result from cancellation of errors. By making comparisons among these two models and derivatives of them, we show that the differences in modeled oxygen and ammonium are largely due to whether or not the BGC codes include cycling of DOM and sedimentary burial of POM, while the differences in modeled nitrate are due to the other differences in the modeled biogeochemical processes (sulfur cycling/anammox/optics). Changes in parameters used in both BGC codes (in particular particle sinking velocities) tended to compensate the other differences. Predictions of hydrogen sulfide (H_2S) within the Bay are very sensitive to the details of the simulation, suggesting that it could be a useful diagnostic.

Key words: Coupled nitrogen and sulfur cycles; Biogeochemical parameters; Model comparison; Predictions of H_2S

1. Introduction

Estuaries are key locations where rivers couple terrestrial processes with ocean biology and chemistry. These systems have generated research interest due to their abundant biological resources and their crucial role in global carbon and biogeochemical cycles (Bauer et al., 2013; Bianchi and Bauer, 2011; Canuel et al., 2012). As the largest estuary in North America, the Chesapeake Bay plays a particularly important role in coastal nutrient transformation, transport and burial. Much effort has been made to study these processes, which can impact the Bay's ecosystem and its economic productivity.

Of all the processes affecting the Bay, eutrophication has emerged as a principal threat. Eutrophication arises from an increase in nutrient and dissolved organic matter (DOM) concentrations, leading to a greater production of particulate organic matter (POM) in the water column or on the seabed (Gary et al., 2002). This results in hypoxia (defined here as oxygen concentrations less than 62.5 $mmol/m^3$) when the oxygen consumed during the degradation of POM exceeds the oxygen supplied from gas exchange, mixing and advection. Hypoxia has been shown to cause mortality events (for recent events within the Chesapeake Bay see Luckett, 2020), contributing to metazoan population decline and resulting in so-called "dead-zones" devoid of fisheries resources including crabs, shrimp and fish (Rabalais et al., 2002; Renaud, 1983).

Under intense hypoxia (as oxygen levels become undetectable), sulfate reduction produces hydrogen sulfide (H_2S) in the water column (a state known as euxinia), which can reduce biodiversity by harming surviving organisms through lethal and sublethal impacts (Luther et al., 1988). Benthic organisms are especially vulnerable to coastal hypoxia, anoxia and euxinia because they live in and near the sediments, where oxygen tends to be depleted relative to the overlying water column (Seliger et al., 1985; Vaquer-Sunyer and Duarte, 2008).

The production of H_2S also has the potential to change biogeochemical cycling in the Chesapeake Bay. Marvin-DiPasquale and Capone (1998) estimated that decomposition of organic matter via sulfate reduction remineralized 18-32% of the primary production at three sites in the Bay. H_2S produced by this process can move upwards in the water column and act as a sink for oxygen when it is oxidized, further accelerating hypoxia (Roden et al., 1992). However, recent work has shown that sulfide can also be oxidized using nitrite and nitrate, resulting in a loss of bioavailable nitrogen (Canfield et al., 2010). Such losses *reduce* the

potential for hypoxia. This process has been referred to as “cryptic" sulfur cycling as sulfide produced from sulfate can be rapidly recycled (and thus may not be detected in the water column on observational time scales). Arora-Williams et al. (2022) find that organisms which are known to have these capabilities are ubiquitous and relatively abundant within the Chesapeake Bay.

Some Chesapeake Bay models (Testa et al., 2014; Cerco and Noel, 2017) incorporate biogeochemical cycling (BGC) codes which have a simplified representation of the impacts of sulfur cycling in which an idealized reductant (representing either H_2S or methane) is released from sediments and oxidized in the water column. However, these models do not directly simulate water column sulfate reduction, sulfide oxidation by nitrate or sulfide oxidation by nitrite.

Other models (for example Feng et al., 2015; Da et al., 2018; Testa et al., 2018) have been able to produce relatively skillful simulations of hypoxia within the Bay using BGC codes that **simulate nitrogen without coupling it to sulfur**. In this paper we use one of these models (the **ChesROMS_ECB** model of Feng et al., 2015 and Da et al., 2018) as our baseline. The physical component of this model is run in the Regional Ocean Modeling System (ROMS; Shchepetkin and McWilliams, 2005), while its biogeochemical component builds on the Fennel et al. (2006) BGC code, which partitions fixed nitrogen between nitrate and ammonium. Feng et al. (2015) add to the Fennel BGC module by including **dissolved organic nitrogen and carbon** and simulating the **burial** of sinking particles in sediment. The resulting model does a relatively successful job in simulating the annual cycle of oxygen in the Bay, but still simulates significant offsets with observations when it comes to nitrate and ammonium (Da et al., 2018).

This raises the question of whether simulating sulfide oxidation by nitrate and nitrite would improve the model or change its sensitivity to perturbations in nitrogen input. In order to examine this question as well as to learn more about nutrient cycles and patterns of hypoxia in the Chesapeake Bay, we implement the BioRedoxCNPS BGC code of **al Azhar et al. (2014),** which **includes sulfur, nitrogen and phosphorus cycles, into the ChesROMS** physical model used in Da et al. (2018). While the BioRedoxCNPS code has many similarities to the ChesROMS_ECB code, it was developed for the open ocean; thus, it **does not include organic matter burial or DOM, and it has a different optics scheme**. Additionally, many processes common to the two codes have **different parameter settings**. While some improvements emerge between the solutions produced by the ChesROMS_ECB and BioRedoxCNPS codes when run in a physically identical simulation of the Chesapeake Bay, it is impossible to tell whether these are due to the inclusion of more complex nutrient cycling, the inclusion of burial and DOM, or to differences in model parameters. To evaluate this, we therefore present a **merged version** of the two codes that includes both the **sulfur and nitrogen cycling** of BioRedoxCNPS and the **burial and dissolved organic matter cycling** of ChesROMS_ECB. This then enables us to isolate sources of differences between the simulations. In what follows we will distinguish between codes, models, and simulations. *Codes* have different representations of biogeochemical or physical processes. *Models* implement these codes in a particular configuration but may produce *simulations* with different values of parameters.

This manuscript is structured as follows. The codes used in this study, the details of how they are implemented into models, and the simulations run with them are described in section 2. We begin our results in section 3 by looking at how the three sets of changes affect predicted oxygen, nitrate and ammonium fields. While the model of al Azhar does produce an improvement in the simulation of oxygen in the Bay, this is not primarily driven by adding sulfur

cycling. Instead, we find that changes in parameters common to both models, as well as the BioRedoxCNPS code's exclusion of burial, DOM cycling, and absorption by CDOM (chromophoric DOM) produced large compensating effects. In Section 4 we discuss implications of these results for modeling the Bay. This study moves towards a more complete model for simulating chemical species and highlights key processes and parameters that control biogeochemical cycles in the Chesapeake Bay. As such our results provide guidance for future experimental studies focused on hypoxia, anoxia and euxinia.

2. Model description

2.1 Physical model

The coupled physical-biogeochemical models used in this study were run with version 3.6 (revision 898) of the Regional Ocean Modeling System (ROMS). ROMS is a three-dimensional, time-dependent simulation that uses the hydrostatic primitive equations (Shchepetkin and McWilliams, 2005). Physical circulations were set to be identical across the different model runs as there was no feedback between biology and physical circulation. While accounting for feedbacks between chlorophyll and shortwave absorption may improve temperature simulations (Kim et al., 2020), ignoring such feedbacks for now allows us to attribute all differences between the models to the direct impacts of biogeochemical processes.

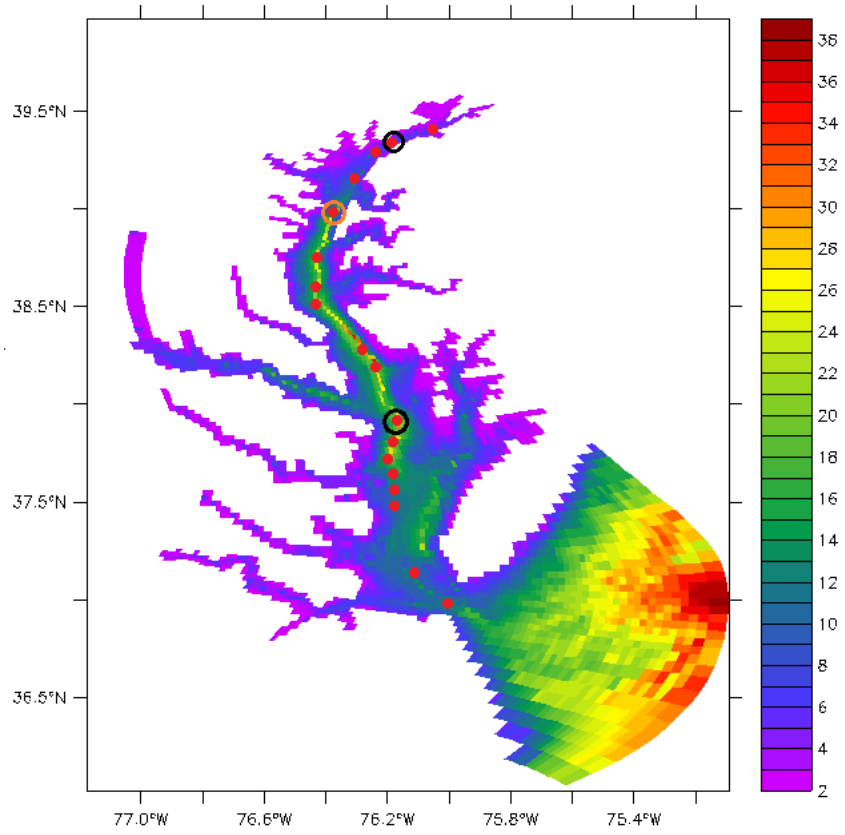

Figure 1. Model bathymetry used in ChesROMS. Stations regularly monitored by the states of Virginia and Maryland are shown in red. In the main text we focus on the CB3.3C station marked with orange circle that is in the heart of the hypoxic zone. In **supplemental material** we also report comparisons from the CB2.2 (near the northern edge of the hypoxic zone) and CB5.3 (near the southern edge of the hypoxic zone) stations marked with black circles.

We use an implementation of the ROMS code for the Chesapeake Bay developed by Xu et al., (2012) and known in the literature as ChesROMS. The ChesROMS model domain extends from 77.2°W to 75.0°W and from 36°N to 40°N, covering the main stem and primary tributaries of the Chesapeake Bay. The model extends seaward to the Mid-Atlantic Bight (Figure 1) to prevent boundary effects from altering tracer fields and mean velocity fields. The horizontal grid uses orthogonal curvilinear coordinates, with varying resolution. The highest resolution (430 m) is found in the northern Bay, the lowest resolution (~10 km) in the southern end of the Mid-Atlantic

Bight, and the average grid spacing within the Chesapeake Bay is 1.7 km. Governing equations are discretized over a stretched terrain-following s-coordinate with 20 vertical levels. To interpolate between a higher resolution in the surface and the bottom boundary layers in deeper waters and relatively constant resolution in shallow waters, the standard stretching function in ROMS was used with values θ_s=6.0 and θ_b=4.0 (standard values in this version of ROMS) with an h_c = 10 m.

Tidal constituents were adopted from the Advanced Circulation (ADCIRC) model (Leuttich et al., 1992) and from observed nontidal water levels from Duck, NC and Lewes, DE (Scully, 2016) and were imposed on the model at the open boundary. Atmospheric forcing, including winds, air temperature, relative humidity, pressure, precipitation, short-wave radiation and longwave radiation, were obtained from the North American Regional Reanalysis (originally described in Mesinger et al., 2006).

The MPDATA 3-D advection scheme (Smolarkiewicz, 1983; Smolarkiewicz and Margolin, 1998) was used for tracers. MPDATA 3-D is a third-order upstream advection scheme that ensures that advection does not generate spurious maxima or minima while minimizing numerical diffusion (this is particularly important for biogeochemical tracers). Momentum is advected with a third-order centered difference scheme in the horizontal and fourth-order centered difference in the vertical. The vertical turbulent mixing scheme and background mixing coefficients for both momentum and tracers were all set to the same values as in Feng et al. (2015).

2.2 BGC codes and simulation setups

In this study, we examined the behavior of three biogeochemical codes (ECB, BioRedoxCNPS, and our merger of the two: SNP_BUR_DOM), which we implemented using two parameter sets

for phytoplankton growth, coagulation and sinking governed by equations in common to the 2 codes. One parameter set is taken from the Da et al. (2018) model of the Chesapeake and the other is taken from the al Azhar et al. (2014) model of the Peru upwelling system. This experimental design thus combines three codes with two parameter sets for each code, giving us a total of six core simulations. In order to highlight the differences between simulations we use a nomenclature that makes it evident what *nutrients* are cycled, whether the model includes *burial and DOM,* and which *parameter set* (Peru vs. Chesapeake) is used within each simulation. The resulting nomenclature shows the increasing complexity and realism in the setup of the simulations.

We denote these simulations N_BUR_DOM_CHES, SNP_PERU, SNP_CHES, N_BUR_DOM_PERU, SNP_BUR_DOM_PERU and SNP_BUR_DOM_CHES. N vs. SNP contrasts whether the code models only Nitrogen (as in ChesROMS_ECB) or Nitrogen, Sulfur and Phosphorus (as in BioRedoxCNPS). BUR_DOM indicates that the code includes organic matter burial in sediments and dissolved organic matter (as in ChesROMS_ECB). Finally, CHES vs. PERU denotes whether the biogeochemical parameters common to both of the two original codes are taken from Da et al. (2018) in the Chesapeake or al Azhar et al. (2014) in the Peru upwelling system. For example, the ChesROMS_ECB model of Da et al. (2018) thus is identical to our N_BUR_DOM_CHES simulation, while the implementation of BioRedoxCNPS with the original parameters used in al Azhar et al. (2014) corresponds to our SNP_PERU simulation. A more complete description of each simulation is given below.

2.2.1 N_BUR_DOM_CHES

The BGC code in the N_BUR_DOM_CHES simulation is the same as the code used in Da et al. (2018), which is derived from a nitrogen-based ecosystem code (Fennel et al., 2006). This code includes a simplified nitrogen cycle with 8 nitrogen pools (and model acronyms): nitrate (NO_3),

ammonium (NH_4), phytoplankton (P), zooplankton (Z), semilabile and refractory dissolved organic nitrogen (DONsl and DONrf) and small and large nitrogen detritus (SDeN and LDeN). Additionally, the code simulates semilabile and refractory DOC (DOCsl and DOCre), inorganic suspended solids (ISS), chlorophyll (Chl), dissolved inorganic carbon (DIC), alkalinity (Alk), and dissolved oxygen (O_2). As implemented in the ChesROMS_ECB model, phytoplankton growth is limited by nitrogen and light and the dominant phytoplankton loss is via coagulation and sinking. Fractions of phytoplankton and large detritus are partially resuspended as small detritus once they reach the bottom, depending on near-bottom turbulent velocities. Some fraction of the remaining benthic flux is buried permanently with the rest being remineralized. The burial fraction f_{bur} follows Henrichs and Reeburgh (1987), where it is a function of the carbon flux to the bottom

$$f_{bur} = \min\left(0.75, 0.023 * carbon\ flux\ to\ the\ bottom^{0.5797}\right) \quad (1)$$

This means that burial is very small when the flux of material is small and increases nonlinearly as the flux to the bottom does. In this model, there are three pathways involved in transforming the organic material to inorganic nitrogen: 1. Solubilization of excreted materials produces DON. Both DON and detrital material are remineralized to NH_4, 2. using oxygen if it is available and 3. nitrate (resulting in denitrification) if it is not. Table S1 lists the biogeochemical parameters used in this simulation. The source of these parameters can be found in Da et al. (2018).

2.2.2 SNP_PERU

The second biogeochemical simulation, SNP_PERU, uses the code developed by al Azhar et al. (2014) to capture interactions between the cycles of nitrogen, phosphorus and sulfur in the Peru coastal ocean upwelling system. Like the ECB code, this code was also derived from the

BGC code of Fennel et al. (2006), and it has previously been referred to as BioRedoxCNPS (al Azhar et al., 2014) and Fennel_CNPS (Hantsoo et al., 2018). We refer to the unaltered version of this code implemented in the ChesROMS physical model domain with BGC parameters from al Azhar et al. (2014) as the SNP_PERU simulation. This code adds new explicit kinetic processes to the Fennel BGC code: 1. Sulfate is reduced to H_2S during organic matter remineralization when other oxidants (oxygen and nitrate) are limiting. Sulfide is reoxidized to sulfate 2. by oxygen, 3. by nitrate reduction to nitrite through chemolithoautotrophic nitrate reduction or 4. by nitrite reduction to N_2 gas through sulfide-driven denitrification. When the water is anoxic, ammonium can also be oxidized by nitrite through anammox to produce N_2 gas. The SNP simulations used in this paper thus include six state variables not included in N_BUR_DOM_CHES: nitrite (NO_2), sulfate (SO_4), hydrogen sulfide (H_2S), phosphate (PO_4) and small and large detrital phosphorus (SDeP, LDeP). Autotrophic nitrogen fixation by diazotrophs (which was included in the original study of al Azhar et al., 2014) was turned off in our simulations as it resulted in numerical instability and is not expected to play a major role in Chesapeake nitrogen dynamics given the excess of fixed nitrogen over phosphorus. It is notable that there are no sedimentary burial processes in the SNP code so that all organic materials hitting the bottom are remineralized. Thus, in comparison to N_BUR_DOM_CHES, SNP_PERU has two new *pathways* (anammox and sulfide-driven denitrification) by which nitrogen is lost to the system, but it simultaneously neglects the loss of nitrogen via burial. Additionally, dissolved organic materials are not included in this model. Finally, as described in Table S1, although the equations for phytoplankton growth, grazing, coagulation, and detrital sinking can be cast in identical forms in SNP_PERU and N_BUR_DOM_CHES, many of the parameters within these equations are different in these two models. In particular, grazing and remineralization rates in N_BUR_DOM_CHES have an exponential dependence on temperature with a Q_{10} of 2.4 taken from Lomas et al. (2002) while those in SNP_PERU do not (corresponding to a Q_{10} of 1).

An additional difference between the N_BUR_DOM_CHES (ChesROMS_ECB) and SNP (BioRedoxCNPS) codes is the parameterization of penetrating photosynthetically active radiation (PAR). In N_BUR_DOM_CHES, PAR is attenuated by water, suspended sediments and implicitly by colored dissolved materials (via a dependence on salinity) but not by chlorophyll. In SNP_PERU it is attenuated by water and chlorophyll alone.

2.2.3 SNP_CHES

With the exception of temperature dependencies for grazing and remineralization, the code in SNP_CHES is the same as in SNP_PERU. However, in any equations which are also in common with N_BUR_DOM_CHES, all common parameters were set to the values in the latter simulation. We also adopted the temperature dependences from the N_BUR_DOM_CHES simulation.

2.2.4 N_BUR_DOM_PERU

In parallel, we ran N_BUR_DOM_PERU by replacing common parameters in the N_BUR_DOM_CHES code with PERU parameters, including setting Q_{10} to 1 for grazing and remineralization. Thus, comparing SNP_PERU (original BioRedoxCNPS) to SNP_CHES (BioRedoxCNPS with parameters from ChesROMS_ECB) or N_BUR_DOM_CHES (original ChesROMS_ECB) to N_BUR_DOM_PERU (ChesROMS_ECB with parameters from BioRedoxCNPS, see Table S1 for list of parameters) helps to distinguish the differences that can be attributed to biological parameters (e.g. phytoplankton growth rate) within identical pathways from the differences caused by changing the biogeochemical pathways themselves (e.g. adding anammox).

2.2.5 SNP_BUR_DOM_PERU

Since the biological model from al Azhar et al. (2014) was developed for an open-ocean/coastal upwelling system rather than an estuary with strong forcing from riverine runoff and significant rates of organic matter burial, we modified the SNP code by adding the resuspension and burial code that was used in ChesROMS_ECB. We also added dissolved organic matter cycling, extending the ECB code which simulated DON and dissolved organic carbon (DOC) to include dissolved organic phosphorus (DOP). Including burial without DOM cycling resulted in an excessive fraction of the nutrients delivered to the model being buried in the river mouths. We denote this merged code as SNP_BUR_DOM, and we denote the simulation made with this new code as SNP_BUR_DOM_PERU when biological constants in common with SNP_PERU are set to those in the latter model.

2.2.6 SNP_BUR_DOM_CHES

For the simulation SNP_BUR_DOM_CHES, the code is identical to that of SNP_BUR_DOM_PERU. However, in those equations which are identical to those in N_BUR_DOM_CHES, all parameters are set to the values in the latter simulation.

2.3 Pairing simulations to isolate sources of the differences between SNP_PERU and N_BUR_DOM_CHES

With our six simulations, we can isolate which differences between SNP_PERU and N_BUR_DOM_CHES contribute to the different simulated results. Differences between SNP_BUR_DOM_PERU and SNP_PERU (or SNP_BUR_DOM_CHES and SNP_CHES) are thus purely due to the inclusion of DOM and burial/resuspension of organic matter. Differences between SNP_BUR_DOM_PERU and N_BUR_DOM_PERU (or SNP_BUR_DOM_CHES and N_BUR_DOM_CHES) are due to differences in whether we include sulfur and phosphorus cycling, or to differences in the optical scheme used to parameterize the penetration of

316 shortwave radiation. Figure 2 shows a schematic of the merged SNP_BUR_DOM code
317 (corresponding to the SNP_BUR_DOM_CHES/PERU simulations). Detailed differences among
318 the six simulations are listed in Table S2.
319
320 2.4 Initial conditions and boundary forcings
321
322 All simulations were run for the year 2017. Riverine inputs for N_BUR_DOM_CHES were taken
323 from the Dynamic Land Ecosystem Model (as in Feng et al., 2015). Tracers found in common
324 across multiple models (ISS, NH_4, NO_3, and DON when included) were set to have the same
325 inputs for SNP_PERU, SNP_CHES, SNP_BUR_DOM_PERU, SNP_BUR_DOM_CHES and
326 N_BUR_DOM_PERU. The riverine input PO_4 was set to be the riverine input NO_3 divided by
327 36.6, a ratio calculated from field data (https://www.chesapeakebay.net/state/pollution). The
328 riverine inputs of SDeP and LDeP were set to the values of SDeN and LDeN divided by 16,
329 respectively, which is the Redfield ratio (reflecting observations of particulate nitrogen and
330 phosphorus within the Bay). Semilabile and refractory DOP were also set to the corresponding
331 DON concentrations divided by 16 when included. Sulfur was not included in the riverine input in
332 this study, consistent with Burke et al. (2018) who found sulfate concentrations in these waters
333 being low (<0.5 mM) compared to much higher concentrations in seawater. At the seaward
334 boundary, we applied a mix of radiative boundary conditions (in which tracers like detrital
335 organic matter are allowed to leave the domain but do not return through the boundary) and
336 radiation with nudging (in which tracers like temperature and salinity entering the domain are set
337 to climatological values). Our new sulfur variables are set to have zero flux on the seaward
338 boundary, which makes little difference on the short time scales for which we run here,
339 especially given the low levels of water column sulfur cycling on the shelf. We will amend this in
340 future iterations of the code. Atmospheric deposition of dissolved inorganic nitrogen (DIN) was

also included in the models as a source of DIN to the estuary, since it is an important fraction of the total DIN inputs to the Chesapeake Bay (Da et al., 2018).

Initial conditions for the N_BUR_DOM_CHES simulation were taken from a previously run ChesROMS_ECB simulation that started in model year 1979 and thus represent a “spun-up” state of the system. Those initial conditions in common with N_BUR_DOM_CHES were set to be the same in SNP_PERU, SNP_CHES, SNP_BUR_DOM_PERU, SNP_BUR_DOM_CHES and N_BUR_DOM_PERU. The initial values of PO_4, SDeP, LDeP, and DOP were all set to be 16 times smaller than their corresponding nitrogen variables from Da et al. (2018). All the other initial values of new state variables were set to zero.

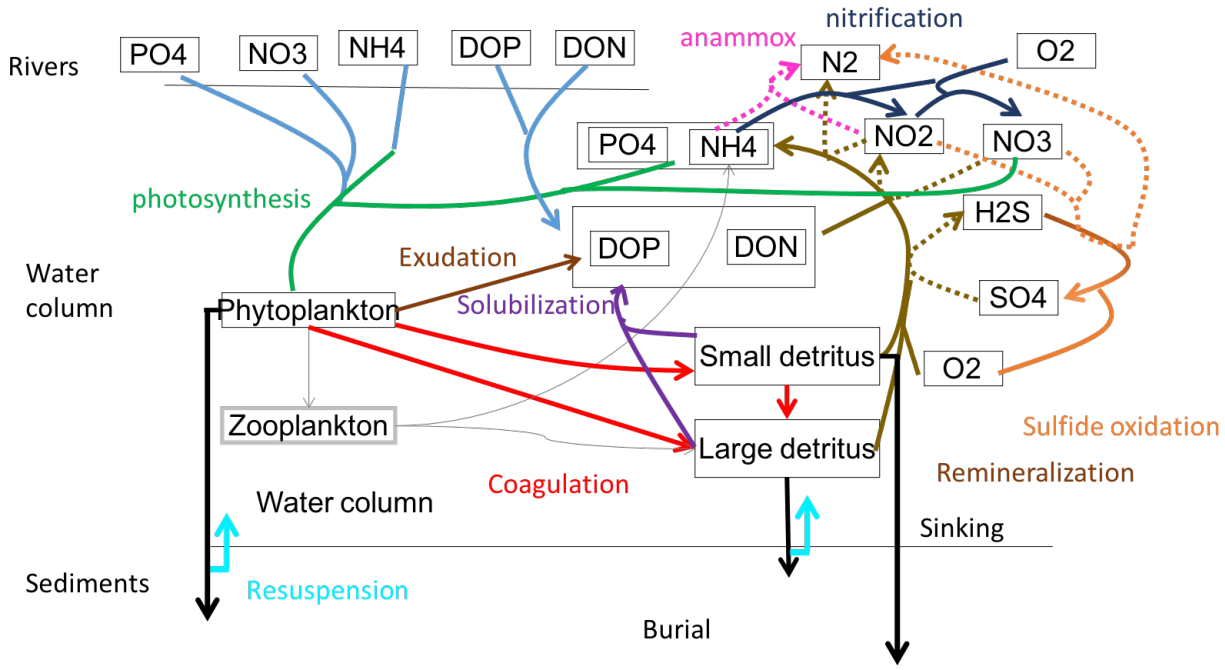

Figure 2. Schematic of the merged biogeochemical code (used in the SNP_BUR_DOM_CHES/PERU simulations) developed in this paper. Nitrate, phosphate and ammonium come down the rivers (light blue lines) and can be taken up by phytoplankton via photosynthesis (green lines). Phytoplankton are primarily lost via coagulation into large and small detritus (red lines) which sink to the bottom. A fraction of phytoplankton and large detritus are partially

resuspended (fluorescent blue lines) as small detritus once they reach the bottom. There is a small loss to zooplankton (grey lines) which we do not focus on here. Detritus is solubilized to DOM (purple lines). Both detritus and DOM can be remineralized (brown lines) to phosphate and ammonium. This remineralization consumes oxygen, but in the absence of oxygen (dotted lines) can proceed using nitrate and nitrite. In the absence of nitrate, nitrite and oxygen, remineralization proceeds using sulfate and produces hydrogen sulfide. Hydrogen sulfide is oxidized back to sulfate (orange lines) using oxygen (solid) or nitrate/nitrite (dotted) with the latter process resulting in denitrification. Ammonium can either be nitrified (dark blue lines) or consumed with nitrite via anammox (dotted magenta lines) in the absence of oxygen.

3. Results

In what follows below, we first compare simulated oxygen, nitrate and ammonium profiles from the simulations of the original BGC codes, N_BUR_DOM_CHES and SNP_PERU, in model year 2017 with the observational data from the Chesapeake Bay Program (CBP, https://www.chesapeakebay.net/what/downloads/cbp_water_quality_database_1984_present). We focus on the annual evolution of these three fields at CB3.3C, a station located near the Chesapeake Bay Bridge in the heart of the hypoxic zone. This station has also been a target of extensive genomic sampling (Arora-Williams, 2020; Arora-Williams et al., 2022), which we will examine in a future manuscript. We also make some comparisons with two other stations, CB2.2 and CB5.3, at the northern and southern edges of the hypoxic zone, respectively. In general, the model does not perform as well at these stations because the annual cycle there is very sensitive to where the edge of the hypoxic zone occurs, and not primarily to the intensity of hypoxia.

We then compare the differences between the SNP and N_BUR_DOM codes (SNP_CHES/PERU versus N_BUR_DOM_CHES/PERU) in order to examine how much of the difference between model fits to the available observations is due to differences in parameters (growth rates, sinking speeds of detritus) that are common to both models. Next, we compare the SNP and SNP_BUR_DOM codes (SNP_CHES/PERU versus SNP_BUR_DOM_CHES/PERU) to examine how adding/removing dissolved organic matter and burial processes affects simulated results. Finally, we show a comparison of N_BUR_DOM and SNP_BUR_DOM codes (N_BUR_DOM_CHES/PERU versus SNP_BUR_DOM_CHES/PERU) to isolate how much of the difference between model fits to the available observations is due to the addition of sulfur and phosphorus cycling and changes in the optics. Note that by definition, the sum of the differences between SNP_PERU minus SNP_BUR_DOM_PERU, SNP_BUR_DOM_PERU minus SNP_BUR_DOM_CHES and SNP_BUR_DOM_CHES minus N_BUR_DOM_CHES add up to the difference between SNP_PERU and N_BUR_DOM_CHES, our two original models. We then evaluate the joint fit of all six simulations to oxygen, ammonium and nitrate. Finally, we present the sensitivity of H_2S to our different model formulations.

3.1 Comparing the base simulations found in the literature：N_BUR_DOM_CHES and SNP_PERU

3.1.1 Qualitative comparison of annual cycle of oxygen at CB3.3C

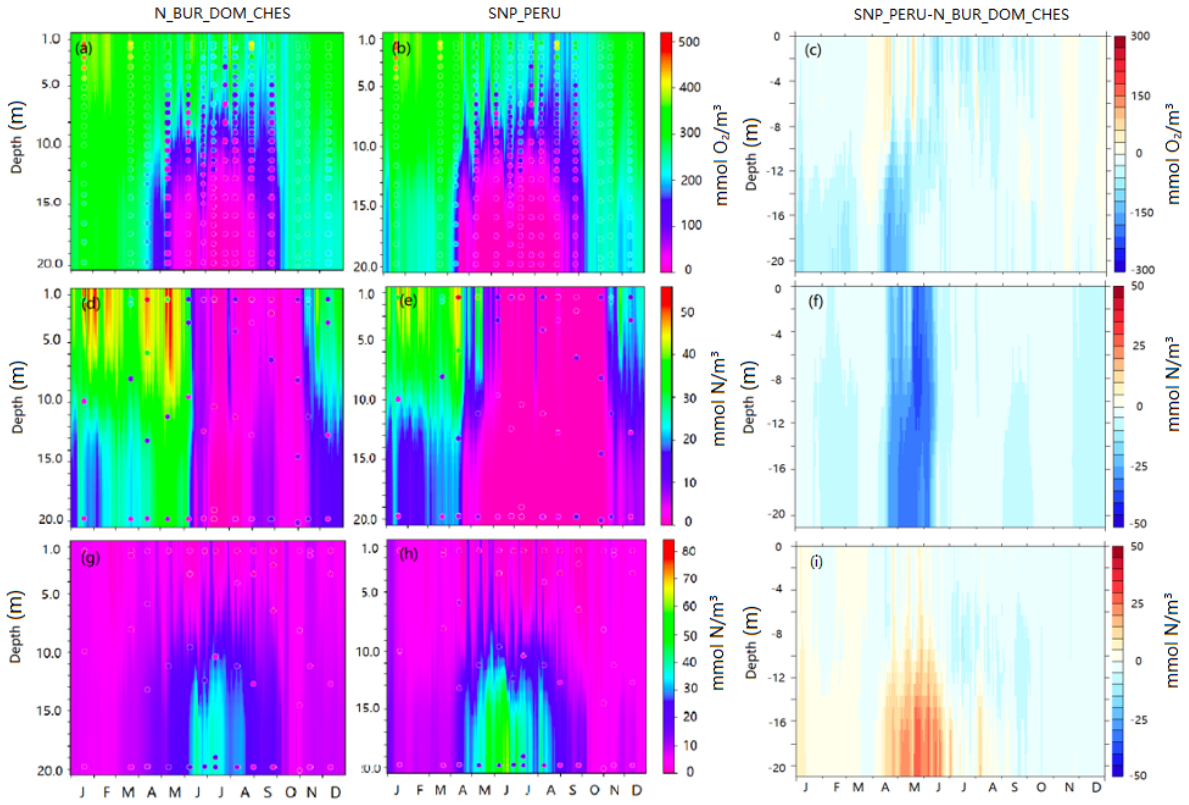

Figure 3. Oxygen (a), (b), Nitrate (d), (e), Ammonium (g), (h) profiles from N_BUR_DOM_CHES (left) and SNP_PERU (right) at the Bay Bridge station (CB3.3C) in year 2017. The colored contours represent model results; the circles represent Chesapeake Bay Program observations. Modeled oxygen (c), nitrate(f) and ammonium (i) difference between SNP_PERU and N_BUR_DOM_CHES at coincident times and locations are shown in the third column.

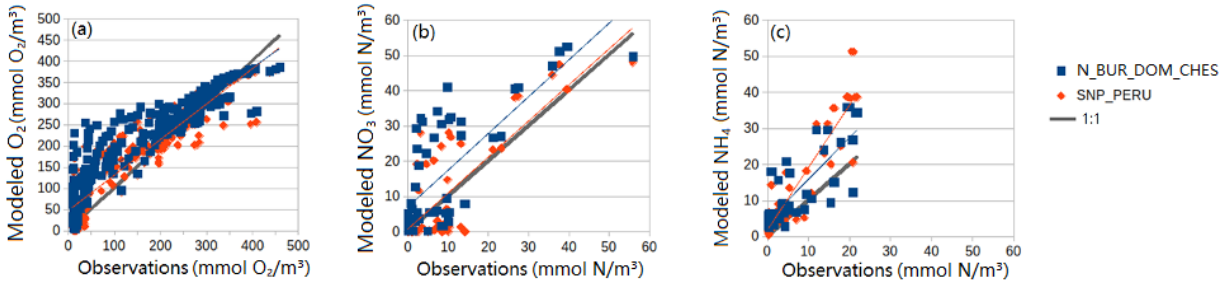

Figure 4. Modeled versus observed oxygen (mmol O_2/m^3) (a), nitrate (mmol N/m^3) (b) and ammonium (mmol N/m^3) (c) at coincident times and locations. Linear fits are shown with colored lines and 1:1 line is shown in black.

Both N_BUR_DOM_CHES and SNP_PERU produce reasonable simulations of oxygen. Figure 3a and 3b show the oxygen concentrations in these two simulations with observations overlaid as colored circles (mismatches can be seen where the circles are visible against the background of the model). N_BUR_DOM_CHES simulates a relatively high oxygen concentration near the surface from January to mid-April, around 350 mmol O_2/m^3. From mid-May to late August, a large hypoxic zone (the so-called dead zone, shown by magenta shading) extends from near the bottom to around 8 m in depth. Around this time period, the oxygen concentration is still high near the surface but decreases rapidly at increasing depths in the water column, corresponding to water column stratification and warming in the Bay during the summer. However, during May and October the observations show noticeably lower oxygen concentration near the bottom than the N_BUR_DOM_CHES simulation does. The SNP_PERU simulation, as shown in Figure 3b, shows a similar distribution of oxygen although the hypoxic zone lasts longer, indicative of earlier onset of hypoxia in 2017.

3.1.2 Quantitative evaluation of model skill in simulating oxygen

Compared to observations, N_BUR_DOM_CHES fits both very low and very high concentrations of oxygen well, but overpredicts intermediate values in the 50-200 mmol/m^3 range (Fig. 4a). SNP_PERU does better in this range. A useful way to objectively compare these fields is the coefficient of determination (referred to as R^2) which can be written as 1-error variance/sample variance. Note that the coefficient of determination can become negative if the error variance exceeds the sample variance; in this sense, it differs from the r^2 produced by a regression model where by definition the error variance is smaller than the sample variance. Both r^2 and R^2 are affected by differences in the pattern of spatiotemporal variation between modeled and predicted fields. However, R^2 also incorporates the contribution to error variance from differences in the mean value and from the amplitude of spatiotemporal variation, and as

such it is a more comprehensive normalized measure of the error. With respect to observed oxygen, SNP_PERU produces a substantial increase in R^2 from 0.72 to 0.85 (Table 1), even though it underpredicts oxygen near the surface. This is because lower observed oxygen concentrations near the bottom are better simulated in SNP_PERU than in N_BUR_DOM_CHES.

3.1.3 Evaluation of the simulations of nitrate and ammonium

Simulations of nitrate from N_BUR_DOM_CHES and SNP_PERU at the Bay Bridge station are shown in Figure 3d and 3e. In the N_BUR_DOM_CHES simulation, the nitrate concentration near the surface is around 40-50 mmol N/m^3 from January to late May with some occasional drops. This is somewhat higher than the observations. Nitrate then drops quickly beginning in early June. The nitrate concentration remains between 0 and 8 mmol N/m^3 throughout the water column during the summer months until early November. The low values are in part due to denitrification removing nitrate in the summer months. In SNP_PERU, the spatiotemporal distribution of nitrate is similar to N_BUR_DOM_CHES from June to November, although the maximum nitrate concentration in the spring is lower, around 48 mmol N/m^3. Depleted nitrate throughout the water column is also observed in this model in the same time period as in N_BUR_DOM_CHES. However, from near the bottom to around 11 m in depth, nitrate decreases in mid-April and remains low until late October. Comparing with observations shows that SNP_PERU more accurately models low nitrate concentrations between around 10 m in depth and the bottom from mid-January to mid-April while results from N_BUR_DOM_CHES are higher than the observations. A scatter plot of nitrate (Figure 4b) also shows that modeled nitrate in SNP_PERU is closer to the observational data, with the linear fit (red line) lying on top of the black 1:1 line, while the linear fit for N_BUR_DOM_CHES is offset above this line. The R^2 for nitrate is much higher in SNP_PERU (0.46) than in N_BUR_DOM_CHES (-0.29), with the

negative value indicating that the RMS error variance is larger than the observational variance at this site.

Figure 3g and 3h compare the simulations of ammonium from N_BUR_DOM_CHES and SNP_PERU. In N_BUR_DOM_CHES, the ammonium concentration from near the bottom to around 10 m in depth begins to increase from mid-April and peaks at 42 mmol N/m^3 in mid-June. Then from late July, it drops gradually and becomes low again in early October. Given that peak values of ammonium between 2015 and 2019 at this site never exceeded 25 mmol N/m^3 we conclude that N_BUR_DOM_CHES predicts too much ammonium during the summer. In SNP_PERU the ammonium concentration near the bottom increases in mid-April and decreases in early September. It peaks at a value of 68 mmol N/m^3 in June. The ammonium-depleted zone near the surface is similar to N_BUR_DOM_CHES. After early September, the ammonium concentration throughout the water column is lower than N_BUR_DOM_CHES. By contrast, in the summer the ammonium concentration in SNP_PERU is about twice that in N_BUR_DOM_CHES. A scatter plot of observed vs. modeled ammonium (Figure 4c) shows that the modeled results of N_BUR_DOM_CHES are closer to the observational data while SNP_PERU gets worse results when it comes to ammonium. The significant overprediction in ammonium means that the R^2 for this variable *decreases* between N_BUR_DOM_CHES (-0.32) and SNP_PERU (-1.12), though clearly errors are large in both simulations. Note, however that the overprediction in SNP_PERU is greatest deep in the water column—there is actually less ammonium above the pycnocline/thermocline/oxycline during the summertime (compare Fig. 3g and h, more blue lines show up above the pycnocline in Fig. 3g, also Fig. 3i).

3.1.4 Annual cycle of differences between the two published models

For most of the year, the oxygen difference between N_BUR_DOM_CHES and SNP_PERU is small, in the range of 0-30 mmol O_2/m^3 (Fig. 3c). From the bottom to around 10 m in depth, SNP_PERU shows obviously lower oxygen than N_BUR_DOM_CHES during middle April to middle May. Near the surface during the same time period, oxygen in SNP_PERU is slightly higher than N_BUR_DOM_CHES. During the summer months near the surface, SNP_PERU shows a lower oxygen concentration.

Nitrate predicted by SNP_PERU is lower than that predicted by N_BUR_DOM_CHES for the whole year (Fig. 3f). Specifically, from middle April to early June, nitrate concentrations in SNP_PERU are much lower than N_BUR_DOM_CHES throughout the water column compared to other times, with differences up to 50 mmol N/m^3. The high nitrate associated with the spring freshet is less persistent in SNP_PERU than in N_BUR_DOM_CHES.

Figure 3i shows the ammonium difference between SNP_PERU and N_BUR_DOM_CHES. SNP_PERU simulates more ammonium than N_BUR_DOM_CHES for the most part from January to August. From middle April to the end of June and from near-bottom to around 10 m in depth, ammonium in SNP_PERU is about 20-30 mmol N/m^3 higher than N_BUR_DOM_CHES. The differences in ammonium have a pattern that is somewhat anticorrelated with the differences in oxygen, suggesting a tradeoff between oxygen and ammonium that we will see more clearly in some of our other simulations.

3.2 Impact of using the PERU parameter set vs CHES parameter set in the 2 BGC codes

While there are many differences between the biogeochemical cycles in the two published codes, parameters such as growth rates and sinking speeds of detritus that are found in both codes also differ. These common parameters would be expected to have effects on our model

results. To quantify this effect, we compare two pairs of models: SNP_PERU minus SNP_CHES (left-hand column of Fig. 5) and N_BUR_DOM_PERU minus N_BUR_DOM_CHES (right-hand column of Fig. 5). This comparison isolates the differences contributed by changing common parameters from their values in Da et al. (2018) to the values in al Azhar et al. (2014) and vice versa. Color scales are the same as in the third column of Fig. 3, enabling a direct comparison of the pattern and magnitude of differences.

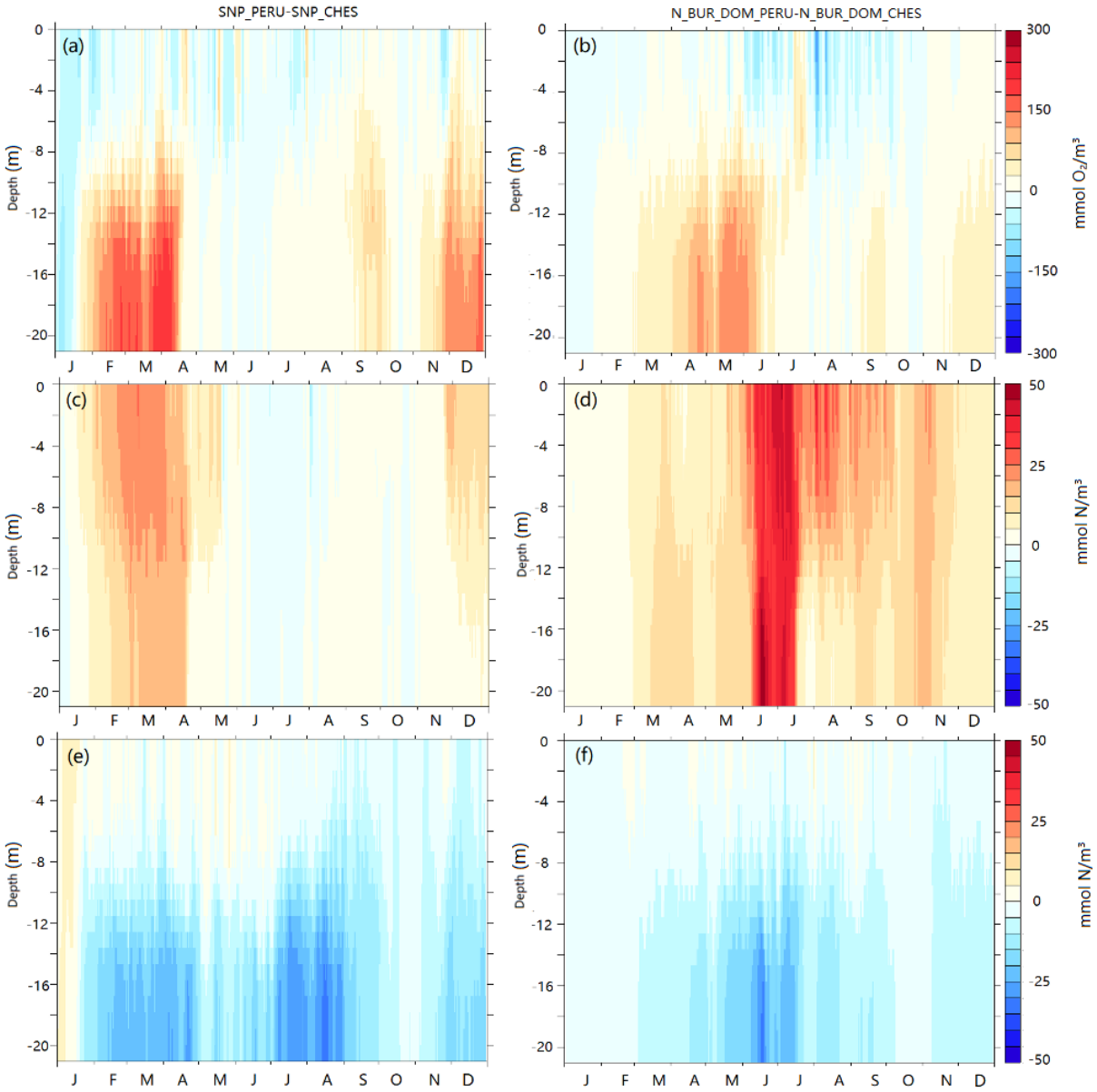

Figure 5. Modeled oxygen (a,b), nitrate(c,d) and ammonium (e,f) for SNP_PERU minus SNP_CHES (left column, a, c and e) and N_BUR_DOM_PERU minus N_BUR_DOM_CHES (right column, b, d and f) at coincident times and locations at the Bay Bridge station (CB3.3C) during 2017.

Switching parameters from CHES values to PERU values does not explain the differences in Fig. 3; in fact, the changes seen have the opposite sign. Qualitatively similar changes are seen in the two pairs of simulations. Oxygen becomes higher from near the bottom to around 8 m in depth. Nitrate gets higher while ammonium becomes lower. SNP_PERU minus SNP_CHES shows more extreme change for oxygen and ammonium with more moderate change for nitrate compared to N_BUR_DOM_PERU minus N_BUR_DOM_CHES. SNP_PERU has much more oxygen than SNP_CHES from late January to middle April and late November to end of December from near the bottom to 10 m in depth, with relative increases of up to 200 mmol O_2/m^3. SNP_CHES extends the hypoxic zone at CB3.3C through much of the year. Oxygen in N_BUR_DOM_PERU is also higher than N_BUR_DOM_CHES during the same time period, consistent with a smaller hypoxic zone shown in time series (Fig. S1 in supplementary materials). In both pairs, using PERU parameters leads to a lower oxygen concentration near the surface, especially during the summer months. From late January to middle April as well as in December, nitrate in SNP_PERU is up to 25 mmol N/m^3 higher than SNP_CHES. This can be explained in terms of the higher levels of oxygen in SNP_PERU reducing denitrification rates, allowing nitrate to persist longer for the PERU parameters relative to the CHES parameters. Nitrate in N_BUR_DOM_PERU is always higher than N_BUR_DOM_CHES, especially from early June to middle July, by up to 50 mmol N/m^3. For ammonium, SNP_PERU is almost always up to 20 mmol N/m^3 lower than SNP_CHES from near the bottom to 10 m in depth, while N_BUR_DOM_PERU is also lower than N_BUR_DOM_CHES but the largest differences appear only in June.

3.3 Measuring the effects of adding BUR and DOM to the SNP code

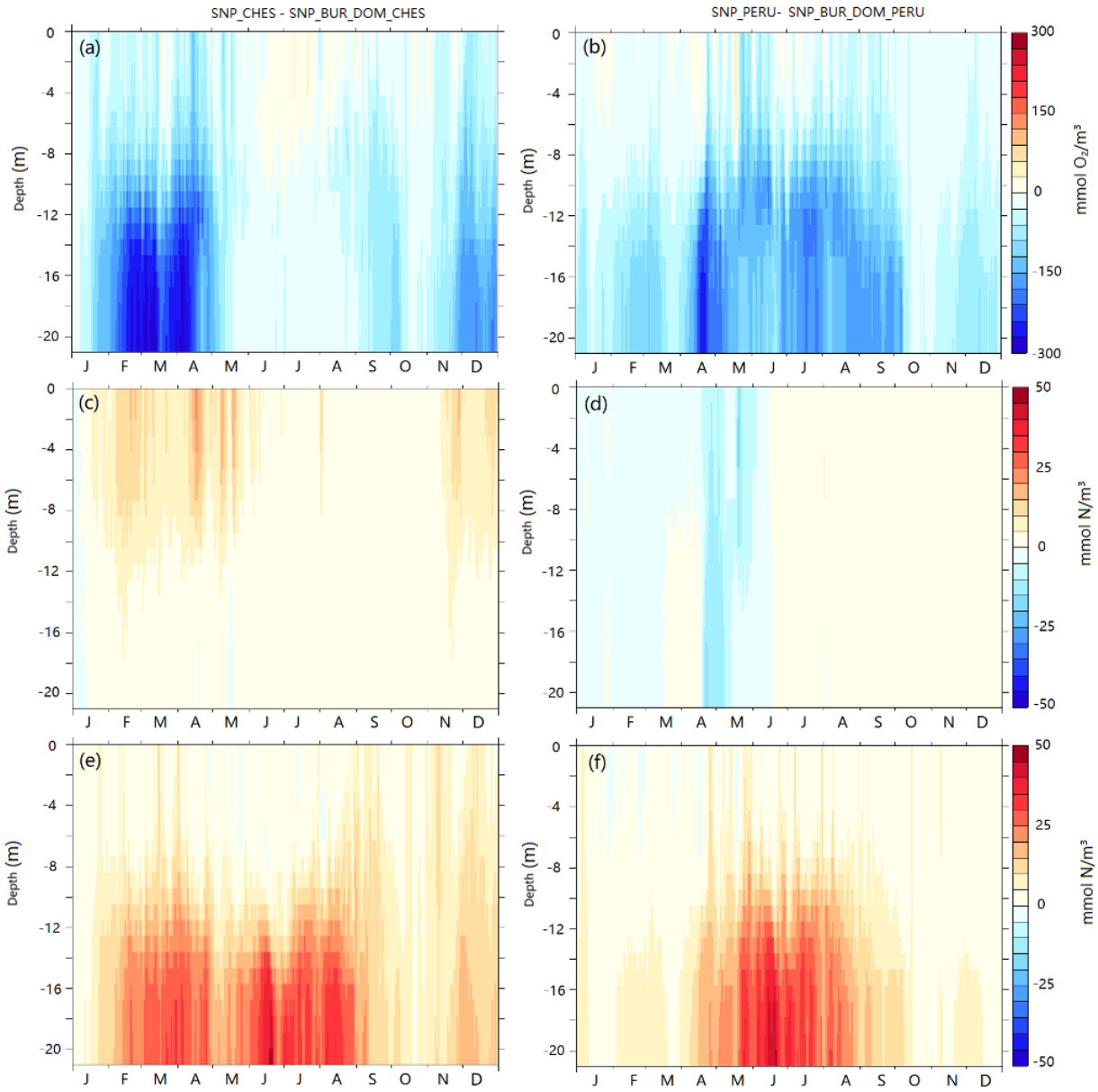

Figure 6. Modeled oxygen (a, b), nitrate (c, d) and ammonium (e, f) for SNP_CHES minus SNP_BUR_DOM_CHES (left column, a, c and e) and SNP_PERU minus SNP_BUR_DOM_PERU (right column, b, d and f) at coincident times and locations at the Bay Bridge station (CB3.3C) during 2017.

Next, we turn to the differences between the simulations induced by adding or removing burial of organic matter and cycling of dissolved organic matter, processes which are not included in the original SNP code of al Azhar et al. (2014). Differences between SNP_CHES versus SNP_BUR_DOM_CHES (left column) and SNP_PERU versus SNP_BUR_DOM_PERU (right column) in oxygen, nitrate and ammonium are shown in Figure 6. We choose to show the impacts of *removing* burial and DOM cycling so as to make it easier to visually attribute the differences between the original models to different sources (we want to know whether the differences between SNP_PERU and N_BUR_DOM_CHES seen in the third column of Fig. 3 are induced by removal of these processes).

For both pairs of simulations, removing dissolved organic matter and burial processes generally more than balances the oxygen and ammonium changes caused by changes in common parameters and thus helps explain the differences seen in Fig. 3. Both pairs of simulations show decreases in oxygen and increases in ammonium concentrations from the bottom to around 8 m in depth, although the time period during which the decrease is seen is different in the two models. Oxygen in SNP_CHES is lower than SNP_BUR_DOM_CHES for most of the year, with significant differences appearing from middle January to early May and late November to late December. During the summer months, oxygen in SNP_CHES is slightly higher than SNP_BUR_DOM_CHES near the surface. Larger difference values for SNP_PERU versus SNP_BUR_DOM_PERU are found from early April to early October. For the most part, surface oxygen concentrations during summertime in SNP_PERU are slightly higher than SNP_BUR_DOM_PERU. SNP_CHES shows much higher values of ammonium than SNP_BUR_DOM_CHES from middle February to late August, while in SNP_PERU the higher values appear from late May to middle August. For nitrate, SNP_CHES is almost always higher than SNP_BUR_DOM_CHES with largest differences appearing near the surface from late January to middle May and middle November to late December. However, from late April to

mid-May nitrate in SNP_PERU is slightly lower than SNP_BUR_DOM_PERU. The differences in nitrate are much smaller than the increases resulting from changing common parameters and so do not explain the differences between the original configurations seen in Fig. 3.

3.4 Direct comparison of the effects of nutrient cycling between the 2 BGC codes: Coupled sulfur, nitrogen and phosphate cycling

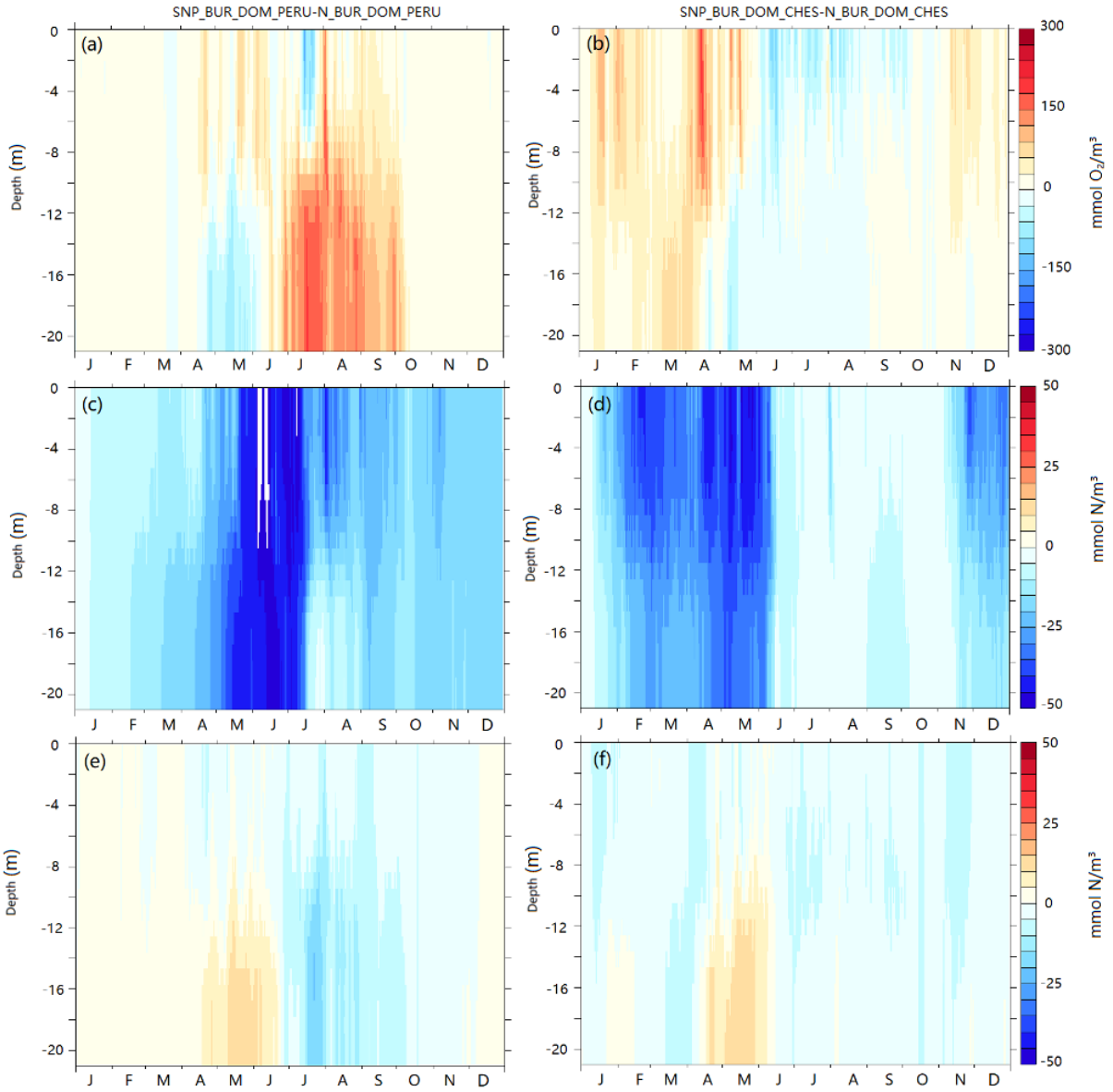

590 Figure 7. Modeled oxygen (a, b), nitrate (c, d) and ammonium (e, f) for SNP_BUR_DOM_PERU
591 minus N_BUR_DOM_PERU (left column, a, c and e) and SNP_BUR_DOM_CHES minus
592 N_BUR_DOM_CHES (right column, b, d and f) at coincident times and locations at the Bay
593 Bridge station (CB3.3C) during 2017.
594
595 We now turn to the differences induced by adding the pathways for sulfur and phosphorus
596 cycling, explicitly modeling nitrite and anammox and changing the optics in al Azhar et al. (2014)
597 but not changing burial or dissolved organic matter cycling. Differences between
598 SNP_BUR_DOM_PERU versus N_BUR_DOM_PERU (left column) and
599 SNP_BUR_DOM_CHES versus N_BUR_DOM_CHES (right column) simulations of oxygen,
600 nitrate and ammonium are shown in Figure 7.
601
602 Adding more complex nutrient cycling and changing the optics produces large decreases in
603 nitrate—explaining why we see decreases in this field in Fig. 3f—but produces smaller changes
604 in oxygen and ammonium. Similar changes for the two pairs of simulations are seen in nitrate
605 and ammonium. Relative to the original ChesROMS_ECB code, the SNP code decreases
606 nitrate concentration: large decreases (up to 50 mmol N/m^3) appear from early May to middle
607 July for SNP_BUR_DOM_PERU minus N_BUR_DOM_PERU, and from late January to early
608 June for SNP_BUR_DOM_CHES minus N_BUR_DOM_CHES. The changes in pathways thus
609 appear to dominate the differences in nitrate seen in Fig. 3. For ammonium,
610 SNP_BUR_DOM_PERU is up to 15 mmol N/m^3 higher than N_BUR_DOM_PERU from early
611 May to early June from bottom to 14 m in depth but up to 30 mmol N/m^3 lower in July. Similar
612 changes can be observed in SNP_BUR_DOM_CHES minus N_BUR_DOM_CHES but the
613 range is less extreme. The changes in nutrient cycling and optics are important for determining
614 the timing of the differences in ammonium seen in Fig. 3 but are not the dominant driver of
615 these differences.

In contrast to nitrate and ammonium, the differences in oxygen induced by adding nutrient cycling and changing the optics depend more on the base simulation. From the bottom to 12 m in depth, oxygen in SNP_BUR_DOM_PERU is lower than N_BUR_DOM_PERU from late April to early June, while from early June to early October, oxygen in SNP_BUR_DOM_PERU becomes higher than N_BUR_DOM_PERU. During the same period and at the same location, SNP_BUR_DOM_CHES and N_BUR_DOM_CHES only exhibit minor differences. During the summer months near the surface, SNP_BUR_DOM_PERU is mostly higher than N_BUR_DOM_PERU while SNP_BUR_DOM_CHES is mostly lower than N_BUR_DOM_CHES. Overall, these differences are smaller than those associated with the previous pairs of experiments.

3.5 Evaluating the accuracy of the model simulations

	R^2/bias for O_2	R^2/bias for NH_4	R^2/bias for NO_3
N_BUR_DOM_CHES	0.72/36.44	-0.32/5.32	-0.29/7.49
N_BUR_DOM_PERU	0.59/41.61	0.27/-0.69	-4.77/24.94
SNP_CHES	0.75/10.66	-8.17/14.14	0.62/-3.19
SNP_PERU	0.85/17.39	-1.13/6.58	0.46/1.08
SNP_BUR_DOM_CHES	0.59/51.23	-0.03/3.14	0.20/-6.02
SNP_BUR_DOM_PERU	0.19/78.95	0.46/-2.28	0.49/0.86

Table 1: Error metrics for the model suite compared with observations. A perfect model would have R^2=1 and bias=0. Values of R^2<0 are associated with large biases, which result in the error variance being larger than the sample variance.

633

634 3.5.1. Statistical analysis: Is there a “best simulation”?

635

636 Examining the R^2 and biases for oxygen, nitrate and ammonium across the models listed in
637 Table 1 demonstrates that the “best” model is not the same for each variable. Large biases play
638 a significant role in decreasing R^2: SNP_CHES has a high ammonium bias of 14.14 with an R^2
639 of -8.17 while N_BUR_DOM_PERU has a high nitrate bias of 24.94 with an R^2 of -4.77. In terms
640 of R^2 averaged across the three variables and also low biases for nitrogen variables,
641 SNP_BUR_DOM_PERU produces the best simulation at CB3.3C. However, the results come at
642 the cost of a degradation of the simulation of oxygen. A tradeoff can be seen between
643 nitrate/ammonium and oxygen simulations among the six simulations. We will return to the
644 implications of this result in the following section.

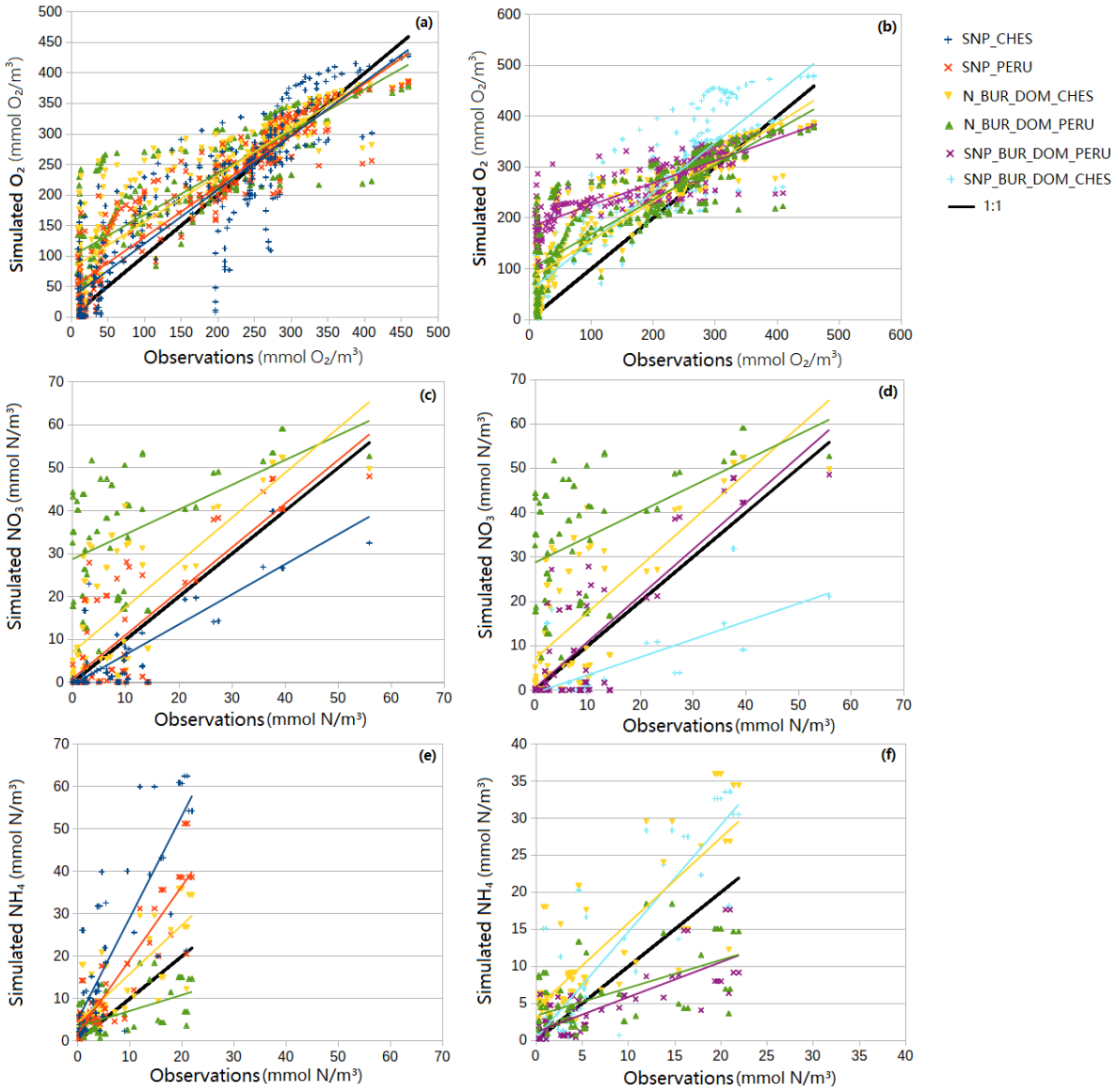

645

646 Figure 8. Simulated versus observed oxygen (mmol O_2/m^3) (a,b), nitrate (mmol N/m^3) (c, d) and
647 ammonium (mmol N/m^3) (e, f) at coincident times and locations from SNP_CHES (blue),
648 SNP_PERU (orange), N_BUR_DOM_CHES (yellow), N_BUR_DOM_PERU (green),
649 SNP_BUR_DOM_PERU (purple) and SNP_BUR_DOM_CHES (light blue). Solid black lines
650 show 1:1 line, colored lines show linear trend. Note that the scales differ between (a) and (b),
651 (e) and (f) in order to make the differences between simulations more visible.

By examining scatter plots comparing observations (horizontal axis) to the modeled values (vertical axis) across these sets of simulations (Figure 8), we can see more details about which mismatches contribute to R^2 difference, and whether this remains consistent across simulations. The top row shows the model-data mismatch for oxygen. We can look at the impact of changing parameter sets by comparing SNP_CHES (yellow, Fig. 8a) with SNP_PERU (orange, Fig. 8a), N_BUR_DOM_CHES (blue, Fig. 8a) with N_BUR_DOM_PERU (green, Fig. 8a) and SNP_BUR_DOM_CHES (light blue, Fig. 8b) with SNP_BUR_DOM_PERU (purple, Fig. 8b). All the models generally overpredict oxygen with the worst mismatch in the 50-200 mmol O_2/m^3 range. Switching from PERU to CHES parameters reduces this mismatch across all three pairs, with the trend lines for SNP_PERU, N_BUR_DOM_PERU and SNP_BUR_DOM_PERU (orange, blue, purple) lying above those for SNP_CHES, N_BUR_DOM_CHES and SNP_BUR_DOM_CHES (yellow, green, light blue). However, at higher values of oxygen the trends reverse. Which parameter set is used modulates the impact of adding new pathways (illustrated in Fig. 8b). SNP_BUR_DOM_PERU has more oxygen at the low end of the range than N_BUR_DOM_PERU but less at the high end, while the reverse is true for SNP_BUR_DOM_CHES with respect to N_BUR_DOM_CHES. Adding dissolved organic matter and burial processes slightly increases the overestimation of oxygen relative to observations in the 50-200 mmol O_2/m^3 range.

For nitrate (middle row) and ammonium (bottom row) the changes are clearer and more consistent across the range of observed values. Holding other factors constant, the PERU parameter set lies above the corresponding CHES parameter set for almost all nitrate samples and below it for almost all ammonium samples. However, for nitrate the ranges over which the changes occur are not the same. N_BUR_DOM_PERU largely increases nitrate at the low end of the range relative to N_BUR_DOM_CHES while the SNP_PERU/SNP_BUR_DOM_PERU simulations see the increase more at the upper end of the range relative to

678 SNP_CHES/SNP_BUR_DOM_CHES. Adding dissolved organic matter and burial processes
679 lowers both the nitrate and ammonium concentrations. Adding pathways generally lowers nitrate
680 (Fig. 8d) and has a relatively small impact on ammonium (Fig. 8f).
681
682 3.5.2 Model predictions of H_2S

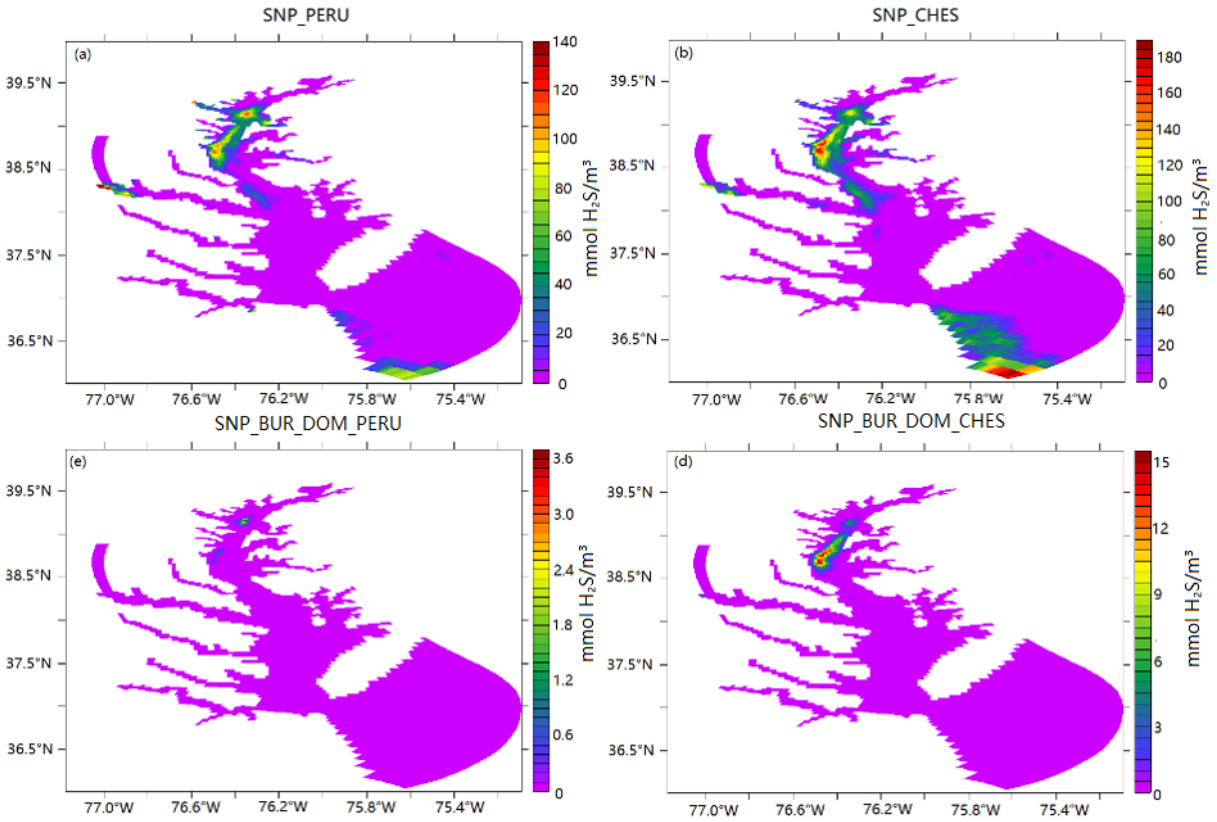

683
684 Figure 9. Simulation of hydrogen sulfide distribution from (a) SNP_PERU (b) SNP_CHES (c)
685 SNP_BUR_DOM_PERU and (d) SNP_BUR_DOM_CHES. Values are averaged in July in 2017
686 and only benthic cells are plotted. Note that the color scales are different in 4 panels-this was
687 done so that the spatiotemporal pattern of the hydrogen sulfide fields could be more easily
688 visualized (enabling us to evaluate whether maxima occurs at the same time and location).
689
690 Our suite of simulations shows wide variation in the predictions of the H_2S concentration. Fig. 9
691 illustrates the sensitivity of simulated bottom water H_2S concentration within

SNP_PERU/SNP_CHES and SNP_BUR_DOM_PERU/SNP_BUR_DOM_CHES. The distribution of maximum H_2S in July is very sensitive to whether organic matter burial and DOM are included in the model. In SNP_PERU, significant levels of H_2S appear in the upper Bay, peaking at 120 mmol H_2S/m^3 along the main stem. In SNP_BUR_DOM_PERU, the zone of euxinia appears in the same region but it is smaller in extent than SNP_PERU, and the peak values are roughly 3.5 mmol H_2S/m^3, nearly two orders of magnitude smaller. SNP_CHES has an even higher peak of H_2S concentration, reaching 160 mmol H_2S/m^3. Adding burial and DON helps lower H_2S in both pairs of simulations, while applying CHES parameters to either code tends to increase H_2S concentration. These results suggest that H_2S could be a sensitive diagnostic for improving models of the Bay.

4 Discussion

In order to develop an understanding of which of the many parameters changed between the models has the biggest impact on model performance, we performed a number of sensitivity studies. Here we report on two that we found to have major impacts on hypoxic volume: particle sinking velocities (i.e., using different sinking velocity constants from CHES versus PERU) and optics (adding or removing CDOM absorption, which is parameterized as a function of DOC). We report on three such simulations here:

1. Starting with SNP_BUR_DOM_PERU, we first reduced the sinking velocities for large and small detritus to those used in the CHES code.
2. We changed the optics scheme of SNP_BUR_DOM_PERU so that CDOM absorption was included.
3. Finally, both changes were added to SNP_BUR_DOM_PERU.

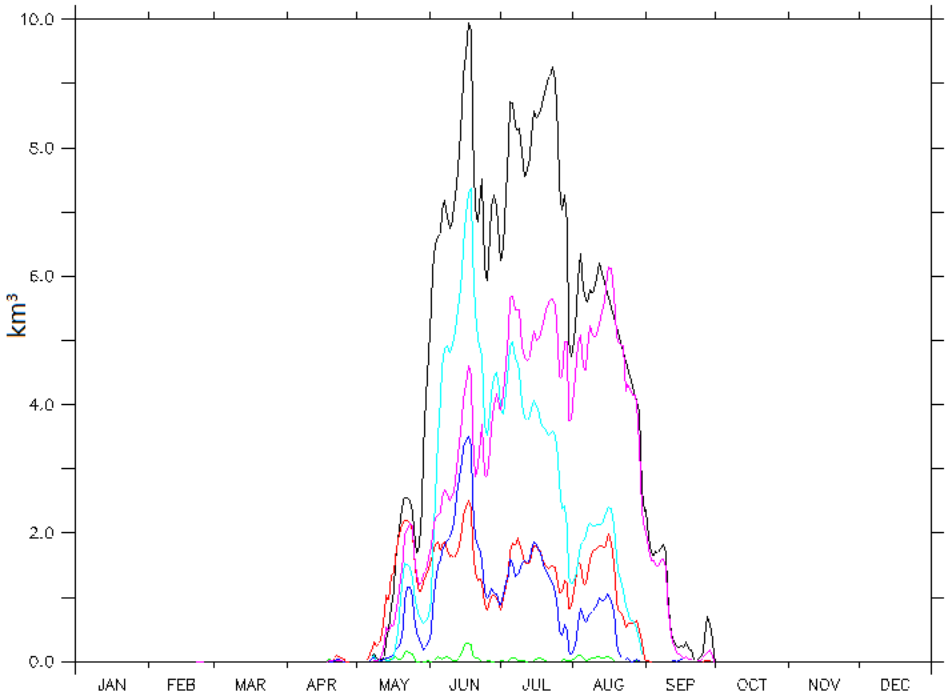

Figure 10. Hypoxic volume (waters with O_2 < 62.5 mmol/m^3) from simulation of N_BUR_DOM_CHES (black), SNP_BUR_DOM_PERU (green), SNP_BUR_DOM_PERU with CHES sinking velocities (red), SNP_BUR_DOM_PERU adding CDOM absorption (dark blue), SNP_BUR_DOM_PERU with CHES sinking velocities and adding CDOM absorption (light blue), SNP_BUR_DOM_CHES (purple)

Both sinking velocity and CDOM absorption impact the volume of hypoxic waters. Figure 10 compares the seasonal evolution of hypoxic volume from these simulations with the hypoxic volume of the original simulation N_BUR_DOM_CHES. In SNP_BUR_DOM_PERU, hypoxia almost vanished (green line) reflecting the high bias seen in Table 1. Decreasing sinking velocities (red) or adding back CDOM absorption (dark blue) resulted in hypoxic volume increasing by roughly the same amount. Changing all the parameters (SNP_BUR_DOM_CHES, purple) but not the optics produces an increase in hypoxia late in the summer. Changing both

732 sinking velocities and optics further increases the hypoxic volume (light blue) to about half the
733 integrated hypoxia of the original simulation (black), with lower hypoxia than
734 N_BUR_DOM_CHES seen late in the summer.
735

CB3.3C	SNP_BUR_DOM_PERU+CDOM absorption with PeruSV/ChesSV	SNP_BUR_DOM_PERU	N_BUR_DOM_CHES
Nitrogen burial	0.1032/0.04001	0.2041	0.0304
Denitrification (sediment)	0.004/0.002	$0.846*10^{-3}$	0.012
Denitrification (water column)	0.095/0.131	0.02525	1.64
Total nitrogen	1.145/1.229	1.042	1.298
reduction of nitrate by sulfide	0.1026/0.1747	0.04615	NA
reduction of nitrite by sulfide	0.09122/0.1244	0.02515	NA
Whole Bay	**SNP_BUR_DOM_PERU+CDOM absorption with PeruSV/ChesSV**	**SNP_BUR_DOM_PERU**	**N_BUR_DOM_CHES**
Nitrogen burial	3.159/1.446	4.736	1.348
Denitrification (sediment)	0.36/0.18	0.039	0.81
Denitrification (water column)	0.089/0.14	0.055	1.015
Total nitrogen	2.72/3.16	2.33	3.02
reduction of nitrate by sulfide	0.146/0.1949	0.11	NA
reduction of nitrite by sulfide	0.086/0.1209	0.054	NA

736

737 Table 2. Nitrogen budget comparisons from (top) CB3.3C and (bottom) the whole Bay. Values
738 shown for CB3.3C are in mol/m^2 while those shown for the whole Bay are in Gmol. Burial,
739 sedimentary denitrification, water column denitrification and reduction of nitrate/nitrite by sulfide
740 represent amounts removed from January through July. Total nitrogen is shown as the vertical
741 integral (at CB3.3C) or volume integral (for the whole Bay) of all living, particulate and dissolved
742 N species averaged from January through July.
743

These changes in results call for a detailed examination of the budget of nitrogen (Table 2). As shown in the lower half of Table 2, compared to N_BUR_DOM_CHES, SNP_BUR_DOM_PERU has significantly more nitrogen burial. This is because the particle sinking velocity determines the particulate flux to the sediments (Eq. 1), such that the higher the sinking velocity, the greater the fraction of primary productivity that is buried. When sinking velocities switch from PERU to CHES (i.e., from high to low), nitrogen burial decreases. This then means that more nitrogen is available to fuel productivity and draw down oxygen.

Including absorption by CDOM also reduces the organic matter burial flux, as this moves primary production up in the water column, allowing more time for remineralization to occur before organic matter hits the sediment. As SNP_BUR_DOM_PERU with CDOM absorption and CHES sinking velocities shows, when both of these processes are added, the total nitrogen inventory for the entire Bay is actually slightly higher than in N_BUR_DOM_CHES (3.16 Gmol vs. 3.02 Gmol). As shown in the top half of Table 2, the corresponding values at CB3.3C qualitatively reproduce the sensitivities for individual loss terms (large relative decrease in water column denitrification and large relative increase in burial for SNP_BUR_DOM_PERU relative to N_BUR_DOM_CHES), but the relative importance of these terms is different at CB3.3C. Because CB3.3C is much deeper (~24 m) than the Bay as a whole, water column remineralization has more time to prevent organic matter from reaching the bottom and being buried.

Table 2 also lists the flux values for sulfur-driven denitrification. Compared to the total N_BUR_DOM_CHES heterotrophic denitrification sink, the autotrophic loss of bioavailable nitrogen via sulfide oxidation in all of the SNP-based models is quite small. On the other hand, when looking only at the results of the SNP models, nitrogen loss via sulfide oxidation is a comparable flux to nitrogen loss through heterotrophic denitrification. For example, in

SNP_BUR_DOM_PERU+CDOM with Chesapeake particle sinking velocities, the whole-Bay flux of nitrate and nitrite reduction by sulfide from January to July in 2017 (0.19 and 0.12 Gmol, respectively) is similar to the heterotrophic denitrification fluxes in the water column and the sediment (0.14 and 0.18 Gmol, respectively). Thus, the SNP simulation results—particularly those with lower particle sinking velocities—suggest that sulfide-driven denitrification could be a significant component of the Chesapeake Bay's nitrogen cycle, a result consistent with the findings in Arora-Williams et al. (2022). However, some caution is warranted in making such an interpretation in light of the large mismatch between the heterotrophic denitrification fluxes in N_BUR_DOM_CHES versus the SNP models.

The denitrification rate in N_CHES_BUR_DOM is further driven up by the larger volume of hypoxic water produced in that simulation. This, in turn, remains a notable difference between N_BUR_DOM_CHES and other simulations (Figure 10), even the SNP_BUR_DOM_CHES simulation, which differs only in terms of the water column remineralization systematics. The discrepancy in hypoxic volume between these two simulations probably results from the different oxic respiration rate coefficients (r) used by the N vs. SNP base models. The N simulations, based on a modification by Da et al. (2018), use a temperature-dependent exponential term for this coefficient such that r = 0.05*exp(0.0742*T), while the SNP simulations use a constant value of r = 0.1. The result is a higher oxic respiration rate in the N-based simulations. At a temperature of 15 ºC, the oxic respiration rate term for the SNP code is still only ~2/3 that of the N code; at 25 ºC, this ratio drops to ~1/2.

	R^2/bias for O_2	R^2/bias for NH_4	R^2/bias for NO_3
SNP_BUR_DOM_PERU with CDOM and PeruSV	0.65/45.23	0.63/-1.35	0.36/3.04

SNP_BUR_DOM_PERU with CDOM and ChesSV	0.70/37.65	0.59/-1.04	0.17/4.68
SNP_BUR_DOM_PERU with ChesSV	0.63/44.95	0.66/1.34	0.39/1.64

Table 3: Error metrics for the model suite compared with observations. A perfect model would have R^2=1 and bias=0.

Picking and choosing which aspects of the ChesROMS_ECB model (N_BUR_DOM) we incorporate into the RedoxCNPS (SNP) model does allow us to improve the joint simulation of nitrogen and oxygen. The R^2 and bias for SNP_BUR_DOM_PERU+CDOM absorption with PeruSV/ChesSV are listed in Table 3. Including CDOM absorption results in a significant increase in R^2 for oxygen and ammonium, but this improvement comes at the cost of slightly reducing R^2 for nitrate. If we were to weight all three fields equally, SNP_BUR_DOM_PERU+CDOM absorption with PeruSV would be chosen as best capturing these three fields.

However, given that oxygen is the field most of interest to Bay water quality managers, we believe that we will need pursue alternative hypotheses to get a simulation that produces comparable improvements in nitrogen species while not compromising the simulation of oxygen. The fundamental tradeoff between oxygen and nitrogen accuracy seen across these simulations suggests that there are also issues with the relationship between them represented by the Redfield ratio. In particular, the stoichiometric ratios used in both of the original codes (O:N of 138:16) are lower than those used in many modern models (Lenton and Watson, 2000; Emerson and Hedges, 1988) with too little oxygen consumed per unit nitrogen added. Preliminary work suggests that changing the stoichiometry of remineralization as well as making the changes we discussed above would generate a simulation which predicts hypoxic volume with comparable skill as N_BUR_DOM_CHES while giving a better prediction for oxygen, nitrate

817 and ammonium. However, full discussion is beyond the scope of this paper where we have
818 chosen to focus on understanding the differences between two published models. We plan to
819 report more fully on this work in a future manuscript.
820
821 We recognize that there are other important differences between the models presented here. In
822 particular, the temperature dependence of the remineralization differs between the
823 N_BUR_DON (ChesROMS_ECB) and the SNP (RedoxCNPS) models, with remineralization
824 rates generally being higher in the former. In the absence of burial, if we decrease the
825 remineralization rates we will increase the PON, partially compensating the decreased
826 remineralization rate. However, decreasing the remineralization rates does allow more of the
827 POM to get transported from the head of the Bay to the deep channel and consume more
828 oxygen there. In the presence of burial, it gets trickier to understand the impact of
829 remineralization rates, because if we decrease the rates, more particulate organic matter
830 survives to hit the sediment. As this means more organic matter is buried we don't increase the
831 organic matter as much because more nutrient is buried and the vertical distribution of nutrients
832 is then different. While changing sinking velocities also changes burial and the vertical
833 distribution of nutrients we have found the resulting changes to nutrient budgets more
834 straightforward to understand. One challenge to investigating the impact of these processes is
835 that they affect small detritus, large detritus and semilabile DON differently, and only total
836 particulate and dissolved nitrogen are currently measured in the Bay.
837
838 **5. Conclusions**
839
840 To date, most models of the Chesapeake Bay have focused on heterotrophic denitrification as
841 the major loss term for fixed nitrogen. While the release of sulfide from sediments has

842 previously been proposed to play an important role in biogeochemical cycling within the
843 Chesapeake Bay (Roden and Tuttle, 1992; Testa et al., 2014; Cerco and Noel, 2017) it has
844 been mostly thought of as a sink for oxygen. However, in recent years it has become clear that
845 other processes, including anammox and cryptic sulfur cycling, can be significant drivers of fixed
846 nitrogen loss in anoxic waters (Canfield et al., 2010). In order to model these additional
847 processes in the Bay, a biogeochemical model for the Peru Upwelling System that included both
848 anammox and sulfide oxidation with denitrification (al Azhar et al., 2014) was implemented in
849 the Bay using the original set of parameters calibrated for the open ocean (SNP_PERU).
850
851 While the SNP_PERU model apparently resulted in an improved simulation for oxygen and
852 nitrate, it did not necessarily do so for the right reasons. Its improvement in modeled oxygen
853 and nitrate concentrations came at the cost of overpredicting the concentration of ammonium.
854 Furthermore, the differences in oxygen concentrations were not driven by the inclusion of new
855 sulfur cycling terms, but rather by the neglect of burial and dissolved organic matter cycling.
856 Omitting organic matter burial and DOM cycling also resulted in increasing the error in
857 ammonium concentrations by allowing ammonium to accumulate in the water column. While
858 differences in nitrate were due to the other differences in equations (sulfur
859 cycling/anammox/optics) we found that optics played an important role in explaining these
860 differences, rather than the inclusion of the cryptic sulfur cycle. Differences in parameters
861 common (PERU vs CHES) to the two codes tended to compensate the other differences, so
862 that using the parameters calibrated for the Chesapeake in the model developed for the open
863 ocean actually made the solution worse. This highlights the extent to which model parameters in
864 Chesapeake Bay models are “best” depends critically which processes are included within the
865 model.
866

867 Our model suite shows a tendency to trade off errors between oxygen and nitrogen species:
868 when the nitrogen simulation gets better, the oxygen simulation gets worse and vice versa. For
869 example, allowing for burial removes nitrogen from the Bay, but if this happens too early in the
870 season, the nitrogen is not present to draw down oxygen in the summer. As noted above, one
871 pathway to address this bias may be the stoichiometric ratio. Alternatively, recent genomic work
872 (Preheim S., S.A. Morris, C. Holder, K. Arora-Williams, Y, Zhang, P. Gensigler, A. Hinton, R.
873 Jin, M.A. Pradal and A. Gnanadesikan, Major trends and environmental correlates of
874 spatiotemporal shifts in the distribution of genes compared to a biogeochemical model
875 simulation in the Chesapeake Bay, manuscript in prep.) suggests that microenvironments
876 (particles, animal guts) may host denitrification in the spring and nitrogen fixation during the
877 summer. Further observational quantification of elemental stoichiometry, as well as the
878 spatiotemporal distribution of nitrification, denitrification and anammox might help to resolve this
879 issue.
880
881 In addition to improving simulations of the seasonal cycling of nitrogen and ammonium, our new
882 SNP_BUR_DOM model allows for predictions of H_2S in the deep Bay (Fig 9). Roden and Tuttle
883 (1992) found the concentration of H_2S is around 6.1 to 27.0 mmol H_2S/m^3 at the mouth of the
884 Choptank River. In Oldham et al. (2015), the concentration ranges more, from 4.28 to 39.7
885 mmol H_2S/m^3 at the Bay Bridge Station. Even higher values of H_2S concentration at the Bay
886 Bridge (up to 60 mmol H_2S/m^3) were reported in Luther et al. (1988). Though we were unable to
887 find measurements of H_2S within the Bay during 2017, our model suite is able to bracket the
888 historical observations. Meanwhile, our simulations show that H_2S is high in SNP_CHES and
889 low in SNP_BUR_DOM_PERU, which suggests that H_2S could be a useful measure of model
890 accuracy.
891

As the most realistic BGC code and parameter setup, our SNP_BUR_DOM code with CDOM absorption and low sinking velocities can serve as a basis for further work. In addition to the changes to O:N stoichiometry alluded to above there are a number of additional biogeochemical phenomena that could be added to the model; sediment processes that we are interested in expanding include cable bacteria which are capable of harvesting electrons from free sulfide in deeper sediment (Malkin and Meysman, 2015) and deposition of organic sulfur in sediments (Jiang et al., 2021). Water column processes include nitrogen fixation by N_2–fixing phytoplankton and heterotrophic bacteria. It is also important to examine whether thresholds for these microbial processes like sulfate reduction are too low as previous work (Arora-Williams et al., 2020; Arora-Williams et al., 2022) shows that genes associated with sulfur cycling may not be limited to the lowest oxygen levels.

Acknowledgement

CJB supported by the Danish National Research Foundation (DNRF 53) toward development of BioredoxCNPS and Villum Foundation (grant 16518) toward KH visiting at UCPH.

Reference

Anderson, L. a, Sarmiento, J.L., 1994. Redfield ratios of remineralization determined by nutrient data analysis. Global Biogeochem. Cycles 8, 65–80. https://doi.org/10.1029/93GB03318

Anderson, L.A., 1995. On the hydrogen and oxygen content of marine phytoplankton. Deep. Res. Part I 42, 1675–1680. https://doi.org/10.1016/0967-0637(95)00072-E

Arora-Williams, K., 2020. Microbial genes, genomes and taxa associated with key aspects of pathogenesis and biogeochemical cycles. Johns Hopkins University.

Arora-Williams, K., Holder, C., Secor, M., Ellis, H., Xia, M., Gnanadesikan, A., Preheim, S.P., 2022. Abundant and persistent sulfur-oxidizing microbial populations are responsive to hypoxia in the Chesapeake Bay. Environ. Microbiol. https://doi.org/10.1111/1462-2920.15976

Azhar, M. Al, Canfield, D.E., Fennel, K., Thamdrup, B., Bjerrum, C.J., 2014. A model-based insight into the coupling of nitrogen and sulfur cycles in a coastal upwelling system. J. Geophys. Res. Biogeosciences 119, 264–285. https://doi.org/10.1002/2012JG002271

Bauer, J.E., Cai, W.-J., Raymond, P.A., Bianchi, T.S., Hopkinson, C.S., Regnier, P.A.G., 2013. The changing carbon cycle of the coastal ocean. Nature 504, 61–70. https://doi.org/10.1038/nature12857

Bianchi, T.S., Bauer, J.E., 2011. Particulate Organic Carbon Cycling and Transformation, in:

925 Treatise on Estuarine and Coastal Science. Elsevier, pp. 69–117.
926 https://doi.org/10.1016/B978-0-12-374711-2.00503-9
927 Burke, A., Present, T.M., Paris, G., Rae, E.C.M., Sandilands, B.H., Gaillardet, J., Peucker-
928 Ehrenbrink, B., Fischer, W.W., McClelland, J.W., Spencer, R.G.M., Voss, B.M., Adkins, J.F.,
929 2018. Sulfur isotopes in rivers: Insights into global weathering budgets, pyrite oxidation,
930 and the modern sulfur cycle. Earth Planet. Sci. Lett. 496, 168–177.
931 https://doi.org/10.1016/j.epsl.2018.05.022
932 Canfield, D.E., Stewart, F.J., Thamdrup, B., De Brabandere, L., Dalsgaard, T., Delong, E.F.,
933 Revsbech, N.P., Ulloa, O., 2010. A Cryptic Sulfur Cycle in Oxygen-Minimum-Zone Waters off
934 the Chilean Coast. Science (80-.). 330, 1375–1378.
935 https://doi.org/10.1126/science.1196889
936 Canuel, E.A., Cammer, S.S., McIntosh, H.A., Pondell, C.R., 2012. Climate Change Impacts on the
937 Organic Carbon Cycle at the Land-Ocean Interface. Annu. Rev. Earth Planet. Sci. 40, 685–
938 711. https://doi.org/10.1146/annurev-earth-042711-105511
939 Carl F. Cerco, M.R.N., 2017. The 2017 Chesapeake Bay Water Quality and Sediment Transport
940 Model. Vicksburg MS.
941 Da, F., Friedrichs, M.A.M., St-Laurent, P., 2018. Impacts of Atmospheric Nitrogen Deposition
942 and Coastal Nitrogen Fluxes on Oxygen Concentrations in Chesapeake Bay. J. Geophys.
943 Res. Ocean. 123, 5004–5025. https://doi.org/10.1029/2018JC014009
944 Devries, T., Deutsch, C., 2014. Large-scale variations in the stoichiometry of marine organic
945 matter respiration. Nat. Geosci. 7, 890–894. https://doi.org/10.1038/ngeo2300
946 Emerson, S., Hedges, J.I., 1988. Processes controlling the organic carbon content of open ocean
947 sediments. Palaeogeogr. Palaeoclimatol. Palaeoecol. 3, 621–634.
948 Feng, Y., Friedrichs, M.A.M., Wilkin, J., Tian, H., Yang, Q., Hofmann, E.E., Wiggert, J.D., Hood,
949 R.R., 2015. Chesapeake Bay nitrogen fluxes derived from a land-estuarine ocean
950 biogeochemical modeling system: Model description, evaluation, and nitrogen budgets. J.
951 Geophys. Res. Biogeosciences 120, 1666–1695. https://doi.org/10.1002/2015JG002931
952 Fennel, K., Wilkin, J., Levin, J., Moisan, J., O'Reilly, J., Haidvogel, D., 2006. Nitrogen cycling in the
953 Middle Atlantic Bight: Results from a three-dimensional model and implications for the
954 North Atlantic nitrogen budget. Global Biogeochem. Cycles 20, n/a-n/a.
955 https://doi.org/10.1029/2005GB002456
956 Gray, J., Wu, R., Or, Y., 2002. Effects of hypoxia and organic enrichment on the coastal marine
957 environment. Mar. Ecol. Prog. Ser. 238, 249–279. https://doi.org/10.3354/meps238249
958 Hantsoo, K.G., Kump, L.R., Haupt, B.J., Bralower, T.J., 2018. Tracking the Paleocene-Eocene
959 Thermal Maximum in the North Atlantic: A Shelf-to-Basin Analysis With a Regional Ocean
960 Model. Paleoceanogr. Paleoclimatology 33, 1324–1338.
961 https://doi.org/10.1029/2018PA003371
962 Henrichs, S.M., Reeburgh, W.S., 1987. Anaerobic mineralization of marine sediment organic
963 matter: Rates and the role of anaerobic processes in the oceanic carbon economy.
964 Geomicrobiol. J. 5, 191–237. https://doi.org/10.1080/01490458709385971
965 Jiang, M., Sheng, Y., Liu, Q., Wang, W., Liu, X., 2021. Conversion mechanisms between organic
966 sulfur and inorganic sulfur in surface sediments in coastal rivers. Sci. Total Environ. 752,
967 141829. https://doi.org/10.1016/j.scitotenv.2020.141829
968 Kim, G.E., St-Laurent, P., Friedrichs, M.A.M., Mannino, A., 2020. Impacts of Water Clarity

969 Variability on Temperature and Biogeochemistry in the Chesapeake Bay. Estuaries and
970 Coasts 43, 1973–1991. https://doi.org/10.1007/s12237-020-00760-x
971 Lenton, T.M., Watson, A.J., 2000. Redfield revisited: 1. Regulation of nitrate, phosphate, and
972 oxygen in the ocean. Regulation 14, 225–248.
973 Lomas, M.W., Glibert, P.M., Shiah, F.-K., Smith, E.M., 2002. Microbial processes and
974 temperature in Chesapeake Bay: current relationships and potential impacts of regional
975 warming. Glob. Chang. Biol. 8, 51–70. https://doi.org/10.1046/j.1365-2486.2002.00454.x
976 Luettich, R.A., Westerink, J.J., Scheffner, N.W., 1992. ADCIRC: An Advanced Three-Dimensional
977 Circulation Model for Shelves Coasts and Estuaries, Report 1: Theory and Methodology of
978 ADCIRC-2DDI and ADCIRC-3DL, Dredging Research Program Technical Report DRP-92-6.
979 Coast. Eng. Res. Cent. (U.S.), Eng. Res. Dev. Cent. (U.S.).
980 Luther, G.W., Church, T.M., 1988. Seasonal cycling of sulfur and iron in porewaters of a
981 Delaware salt marsh. Mar. Chem. 23, 295–309. https://doi.org/10.1016/0304-
982 4203(88)90100-4
983 Malkin, S.Y., Meysman, F.J.R., 2015. Rapid Redox Signal Transmission by “Cable Bacteria”
984 beneath a Photosynthetic Biofilm. Appl. Environ. Microbiol. 81, 948–956.
985 https://doi.org/10.1128/AEM.02682-14
986 Marvin-DiPasquale, M., Capone, D., 1998. Benthic sulfate reduction along the Chesapeake Bay
987 central channel. I. Spatial trends and controls. Mar. Ecol. Prog. Ser. 168, 213–228.
988 https://doi.org/10.3354/meps168213
989 Mesinger, F., DiMego, G., Kalnay, E., Mitchell, K., Shafran, P.C., Ebisuzaki, W., Jović, D., Woollen,
990 J., Rogers, E., Berbery, E.H., Ek, M.B., Fan, Y., Grumbine, R., Higgins, W., Li, H., Lin, Y.,
991 Manikin, G., Parrish, D., Shi, W., 2006. North American Regional Reanalysis. Bull. Am.
992 Meteorol. Soc. 87, 343–360. https://doi.org/10.1175/BAMS-87-3-343
993 N.Luckett, C., 2020. 2019 Fish Kill Summary.
994 Oldham, V.E., Owings, S.M., Jones, M.R., Tebo, B.M., Luther, G.W., 2015. Evidence for the
995 presence of strong Mn(III)-binding ligands in the water column of the Chesapeake Bay.
996 Mar. Chem. 171, 58–66. https://doi.org/10.1016/j.marchem.2015.02.008
997 Rabalais, N.N., Turner, R.E., Wiseman, W.J., 2002. Gulf of Mexico Hypoxia, A.K.A. “The Dead
998 Zone.” Annu. Rev. Ecol. Syst. 33, 235–263.
999 https://doi.org/10.1146/annurev.ecolsys.33.010802.150513
1000 Renaud, M.L., 1983. Hypoxia in Louisiana Coastal Waters during 1983: Implications for Fisheries.
1001 Fish. Bull. 84, 19–26.
1002 Roden, E.E., Tuttle, J.H., 1992. Sulfide release from estuarine sediments underlying anoxic
1003 bottom water. Limnol. Oceanogr. 37, 725–738. https://doi.org/10.4319/lo.1992.37.4.0725
1004 Scully, M.E., 2016. Mixing of dissolved oxygen in Chesapeake Bay driven by the interaction
1005 between wind-driven circulation and estuarine bathymetry. J. Geophys. Res. Ocean. 121,
1006 5639–5654. https://doi.org/10.1002/2016JC011924
1007 Seliger, H.H., Boggs, J.A., Biggley, W.H., 1985. Catastrophic anoxia in the Chesapeake Bay in
1008 1984. Science (80-.). 228, 70–73. https://doi.org/10.1126/science.228.4695.70
1009 Shchepetkin, A.F., McWilliams, J.C., 2005. The regional oceanic modeling system (ROMS): a
1010 split-explicit, free-surface, topography-following-coordinate oceanic model. Ocean Model.
1011 9, 347–404. https://doi.org/10.1016/j.ocemod.2004.08.002
1012 Smolarkiewicz, P.K., 1983. A Simple Positive Definite Advection Scheme with Small Implicit

Diffusion. Mon. Weather Rev. 111, 479–486. https://doi.org/10.1175/1520-0493(1983)111<0479:ASPDAS>2.0.CO;2

Smolarkiewicz, P.K., Margolin, L.G., 1998. MPDATA: A Finite-Difference Solver for Geophysical Flows. J. Comput. Phys. 140, 459–480. https://doi.org/10.1006/jcph.1998.5901

Testa, J.M., Kemp, W.M., Boynton, W.R., 2018. Season-specific trends and linkages of nitrogen and oxygen cycles in Chesapeake Bay. Limnol. Oceanogr. 63, 2045–2064. https://doi.org/10.1002/lno.10823

Testa, J.M., Li, Y., Lee, Y.J., Li, M., Brady, D.C., Di Toro, D.M., Kemp, W.M., Fitzpatrick, J.J., 2014. Quantifying the effects of nutrient loading on dissolved O2 cycling and hypoxia in Chesapeake Bay using a coupled hydrodynamic-biogeochemical model. J. Mar. Syst. 139, 139–158. https://doi.org/10.1016/j.jmarsys.2014.05.018

Vaquer-Sunyer, R., Duarte, C.M., 2008. Thresholds of hypoxia for marine biodiversity. Proc. Natl. Acad. Sci. 105, 15452–15457. https://doi.org/10.1073/pnas.0803833105

Xu, J., Long, W., Wiggert, J.D., Lanerolle, L.W.J., Brown, C.W., Murtugudde, R., Hood, R.R., 2012. Climate Forcing and Salinity Variability in Chesapeake Bay, USA. Estuaries and Coasts 35, 237–261. https://doi.org/10.1007/s12237-011-9423-5